Sigma-Delta-over-Fiber for High-Speed Wireless Communication Systems

IBRAHIM CAN SEZGIN

CHALMERS

Sigma-Delta-over-Fiber for High-Speed Wireless Communication Systems

Ibrahim Can Sezgin

Abstract

Future mobile communication networks aim to increase the communication speed, provide better reliability and improve the coverage. It needs to achieve all of these enhancements, while the number of users are increasing drastically. As a result, new base-station (BS) architectures where the signal processing is centralized and wireless access is provided through multiple, carefully coordinated remote radio units are needed.

The sigma-delta-over-fiber (SDoF) is a communication technique that can address both requirements and enable very low-complexity, phase coherent remote radio transmission, while transmitting wide-band communication signals with high quality. This thesis investigates the potential and limitations of SDoF communication links as an enabler of future mobile networks.

In the first part of the thesis, a multiple-input-multiple-output (MIMO) communication testbed with physically separated antenna elements, distributed-MIMO, is formed by multiple SDoF links. It is shown that the digital up-conversion, performed with a shared local-oscillator/clock at the central unit, provides excellent phase coherency between the physically distributed antenna elements. Moreover, the same approach decreases the complexity and the package size of the antenna units significantly by moving the complexity of the BSs to a central unit. The implemented testbed is evaluated through various communication experiments. The results show that distributing the antenna units of a MIMO communication system can increase the coverage and signal quality.

In the second part of the thesis, an ultra-high-speed SDoF (UHS-SDoF) link is realized by using the state-of-the-art vertical-cavity surface-emitting-lasers (VCSEL). The effects of VCSEL characteristics on such links in terms of signal quality, energy efficiency and potential lifespan is investigated. Furthermore, the potential and limitations of UHS-SDoF are evaluated with signals having various parameters. The results show that, low-cost, reliable, energy efficient, high signal quality SDoF links can be formed by using emerging VCSELs. Therefore, UHS-SDoF is a very promising technique for beyond 10 GHz communication systems.

In conclusion, this thesis has showed that low-complexity, low-cost, and energy efficient ultra-high speed communication links and distributed MIMO systems can be implemented by employing SDoF.

Keywords: Sigma-delta-over-fiber (SDoF), distributed-MIMO, vertical-cavity surface-emitting-laser (VCSEL), ultra-high speed communication.

List of Publications

Appended Publications

This thesis is based on work contained in the following papers:

[A] I. C. Sezgin, M. Dahlgren, T. Eriksson, M. Coldrey, C. Larsson, J. Gustavsson, and C. Fager, "A low-complexity distributed-MIMO testbed based on high-speed sigma-delta-over-fiber," to appear in *IEEE Trans. Microw. Theory Techn.*, 2019.

[B] I. C. Sezgin, T. Eriksson, J. Gustavsson, and C. Fager, "Evaluation of distributed MIMO communication using a low-complexity sigma-delta-over-fiber testbed," accepted for presentation at *IEEE MTT-S Int. Microw. Symp. Dig.*, Jun. 2019.

[C] I. C. Sezgin, J. Gustavsson, T. Lengyel, T. Eriksson, Z. H. Se, and C. Fager, "Effect of VCSEL characteristics on ultra-high speed sigma-delta-over-fiber communication links," *J. Lightw. Technol.*, pre-print, 2019, doi: 10.1109/JLT.2019.2898270.

[D] I. C. Sezgin, T. Eriksson, J. Gustavsson, and C. Fager, "A flexible multi-Gbps transmitter using ultra-high speed sigma-delta-over-fiber," in *IEEE MTT-S Int. Microw. Symp. Dig.*, pp. 1195–1198, Jun. 2018, doi: 10.1109/MWSYM.2018.8439200.

Abbreviations

5G	Fifth Generation Mobile Networks
AP	Access Point
ARoF	Analog-Radio-over-Fiber
CFO	Carrier-frequency Offset
CFP	C-form-factor Pluggable Transceiver
CPRI	Common Public Radio Interface
CSI	Channel State Information
CU	Center Unit
DAC	Digital-to-Analog Converter
DSP	Digital Signal Processing
DRoF	Digital-Radio-over-Fiber
EAM	Electro-absorption Modulator
EVM	Error Vector Magnitude
FPGA	Field-programmable Gate Array
HBR	Heat-to-bitrate Ratio
IF	Intermediate Frequency
IMD	Intermodulation Distortion
LNA	Low-noise Amplifier
LO	Local Oscillator
MIMO	Multiple Input Multiple Output
MMF	Multi-mode Fiber
NTF	Noise Transfer Function
OBSAI	Open Base Station Architecture Initiative
OSR	Oversampling Ratio
PA	Power Amplifier
RAM	Random-access-memory
RoF	Radio-over-Fiber
PPG	Pulse-pattern Generator
RF	Radio Frequency
RU	Remote Unit
SDM	Sigma Delta Modulation
SDoF	Sigma-Delta-over-Fiber
SIR	Signal-to-interference Ratio
SFP	Small Form-factor Pluggable Transceiver

SMF	Single-mode Fiber
SNR	Signal-to-noise Ratio
STF	Signal Transfer Function
VCSEL	Vertical-Cavity Surface-Emitting-Lasers

Contents

Chapter 1

Introduction

Our lives are changing dramatically with the development of communication technology. Almost without any effort, just by using your phone, you can socialize with your friends, let your friends see what you are eating, check your emails, watch an ultra-high-definition (UHD) movie while travelling, pay your bills, surf through the limitless world of the Internet. It has become obsolete to carry a map of the city your are travelling or a dictionary when you are abroad. You need only one thing: your mobile phone with internet access.

All these charming benefits of mobile internet access attract more and more users. In 2018, 240 million new subscriptions are made to mobile broadband services globally [1]. Today, there are more than 5.7 billion mobile broadband subscriptions, globally, and it is expected to increase to 8.4 billion by the year 2024. The average monthly data traffic per subscription is expected to increase from 5.6 gigabytes (GB) to 21 GB in this time period, corresponding to a total data traffic increase from 27 exabyte (EB) to 136 EB per month [1].

The communication speed has grown exponentially during the evolution of mobile communication technology. The second generation mobile communication technology (2G) was able to transmit 64 kbps in 1990s. In 2004 a maximum data rate of 2 Mbps was available with the third generation mobile system (3G). Today, a mobile phone can communicate at a date rate between 200 Mbps and 1 Gbps thanks to the fourth generation mobile system (4G). The latest mobile system technology 5G, which is currently being deployed, is expected to provide data rates higher than 1 Gbps [1].

These high speed communications and the new life style of *always being connected* are enabled by a wireless communication link between a mobile phone and a base-station (BS). In a nutshell, when a user wants to transmit and/or receive data, his or her mobile phone communicates through an antenna located at a base-station tower. Thereafter, the information received by the antenna is transferred to a base-station control unit located close to the tower. The communication link between the antenna and the base-station control unit can be formed either by electrical or optical cables. The previously mentioned constant demand of higher data rates and increased coverage requires major improvements of these links between the antenna and the control unit in a base-station. Radio-over-fiber (RoF) is a technique to realize these links with optical fiber cables. Radio-over-fiber (RoF) is already a standardized approach to form such links and is a strong candidate as an enabling technique for 5G [2].
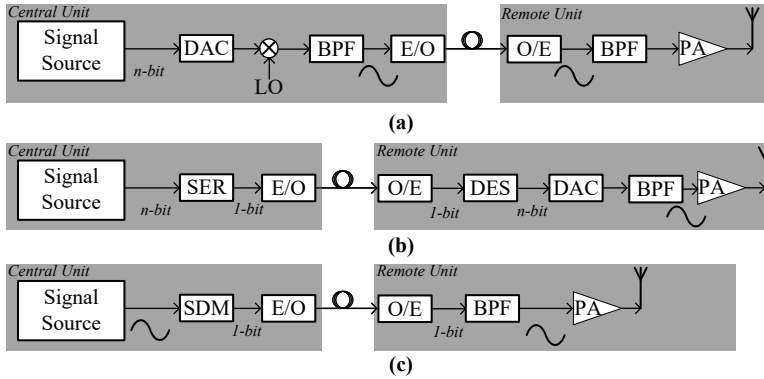
Figure 1.1: General structure of ARoF (a), DRoF (b), and SDoF (c). DAC: Digital to Analog Converter, BPF: Bandpass Filter, E/O: Electrical to Optical Converter, O/E: Optical to Electrical Converter, PA: Power Amplifier, SER: Serializer, DES: Deserializer, SDM: Sigma Delta Modulator.

1.1 Radio-over-Fiber

Utilizing optical fibers to distribute radio communication was first proposed in the 1990 [3,4]. Since then, it has been developing rapidly and today it is used in many different areas including: radio signal distribution, electronic warfare, terahertz spectrescopy [5]. The main advantage of RoF, is exploiting the low-loss and wide bandwidth nature of optical communication to distribute high frequency radio signals over a large distance.

The RoF technique simplifies the conventional BSs by shifting the main operations of it to a central unit, which communicates with multiple BSs [6]. In RoF, an electrical radio signal modulates the optical source, thereafter an optical fiber transports the optical signal to a remote unit, where it is converted back to the electrical domain with a photo detector. The optical fiber provides a low attenuation and interference free communication medium. The RoF technique has different variants, each with different advantages and disadvantages. Below, the three most common implementations are discussed.

1.1.1 Analog-Radio-over-Fiber

The traditional implementation of RoF utilizes analog modulation, and is therefore called analog-radio-over-fiber (ARoF) [7–12]. In ARoF, a digital communication signal is transformed to an analog signal by a digital-to-analog converter (DAC), see Fig 1.1 (a). After that, the analog signal, is generally up-converted to a carrier frequency prior to the electrical to optical conversion. The up-converted electrical signal drives an optical source, which is followed by an optical fiber. At the far end of the fiber, the electrical signal is recovered with a photo-diode. After that the electrical signal is filtered, amplified and finally transmitted over the air by an antenna.

As illustrated in Fig 1.1 (a), the up-conversion stage at the central unit simplifies the remote unit by eliminating the local-oscillator and mixer stages in it. However, using this method for transmission of up-converted signals requires an optical laser capable of generating high-speed optical signals and a

photodetector directly generating the corresponding electrical signal. Designing such components is not an easy task. Furthermore, designing these components becomes more challenging as the carrier frequency increases [13].

Another main limitation of ARoF is the nonlinearities of the optical components, e.g. laser, photodetector, resulting in inter-modulation distortion (IMD) [14]. In [15] it is shown that these non-linearities are the main performance limitation of ARoF communication links, since it effects the dynamic range of the link. Furthermore, the chromatic dispersion effect of optical fiber is another disadvantage of ARoF, especially for mm-wave communication systems with ultra-wide bandwidth signals [16].

An method to mitigate the chromatic dispersion and the requirement of high-speed optical components is to transmit baseband or intermediate-frequency (IF) signals over the fiber [13]. However, this technique increases the complexity of the remote unit due to performing the up-conversion stage at the remote unit.

1.1.2 Digital-Radio-over-Fiber

An alternative to ARoF is to transmit digital signals in the optical channel, rather than analog ones. This technique is called digitized-radio-over-fiber (DRoF) [17, 18]. DRoF is a standardized communication method for cellular networks, e.g. open base station architecture initiative (OBSAI) [19] and common public radio interface (CPRI) [20] . In DRoF communication scheme, a serialized digital signal is transmitted, see Fig 1.1 (b). The digital signal modulates an optical laser, which is followed by an optical fiber. At the remote unit, the optical signal is converted back to electrical domain and de-serialized. Thereafter, the digital signal is transformed to an analog signal with a high-bandwidth DAC. Finally, the electrical signal is filtered, amplified and transmitted over the air by an antenna.

If the up-conversion stage is performed at the remote unit, the complexity of it increases. On the other hand, the small fractional bandwidths of most common wireless standards, (e.g. WI-FI, 3G, 4G), relative to their carrier frequencies, enable to use bandpass sampling techniques [17, 21]. In this way, the sampling rate requirements of of the DAC decreases drastically, since bandpass sampling enables to sample a signal with a frequency much lower than its Nyquist rate. Overall, the digital signal transmission eliminates the non-linearity and dynamic range limitation of ARoF [22] at the cost of employing a high-bandwidth, expensive, power hungry DAC at the remote unit.

1.1.3 Sigma-Delta-over-Fiber

Another technique to realize RoF links is sigma-delta-over-fiber (SDoF). It offers advantages over both ARoF and DRoF [23]. Similar to DRoF, it utilizes a digital-optical link between the central and remote unit, see Fig. 1.1 (c). Hence, it has the previously mentioned benefits of DRoF in terms of non-linearity and dynamic range. Moreover, the sigma-delta modulator eliminates the DAC from the remote unit, since the analog signal can be recovered only with a bandpass filter. The digital up-conversion stage at the central unit provides a very low-complexity remote unit.

1.2   Thesis Contribution and Outline

In this thesis, potential and limitations of sigma-delta-over-fiber communication links are investigated. Chapter 2, starts with an introduction to sigma-delta modulation, followed by various implementation types. The advantages and limitations of different variants of SDoF communication schemes depending on the band of operation are also presented.

Chapter 3 focuses on centralized structure of SDoF, and presents a fully synchronized multi antenna wireless communication system testbed. The proposed testbed in [Paper A], employs an all-digital sigma-delta-over-fiber architecture to generate and distribute RF communication signals from single central station to multiple spatially distributed remote units, using standard FPGA and high-speed digital optical interconnect components. Centralized structure provides excellent phase coherency between physically distributed remote units. Furthermore, it decreases the complexity and the cost of remote units significantly, while enabling a highly flexible testbed due to the all-digital structure. Various multi antenna system experiments are performed with the proposed testbed and the results are presented [Paper B].

In Chapter 4, the focus is on the limitation and potentials of a single SDoF communication link. In order to discover these, an ultra-high speed SDoF link is formed by state-of-the-art vertical-cavity surface-emitting-lasers (VCSEL). The effects of the laser characteristics on such links are evaluated by various experiments [Paper C]. The potential and limitations of SDoF at carrier frequencies beyond 10 GHz for transmission of wideband modulated signals are also investigated [Paper D].

In the final chapter, the future and the outcomes of the presented work is presented.

Chapter 2

Sigma-Delta-over-Fiber

Sigma-delta-over-fiber (SDoF) is a variant of radio-over-fiber, which employs sigma-delta modulation (SDM) in order to generate and transmit digital signals with few discrete amplitude levels thru optical fiber. The key aspect of SDoF communication is transmission of a digital signal, which carries a modulated RF-signal. Similar to DRoF, digital signal transmission is immune to non-linearities [23]. On contrary, the power-hungry, high-bandwidth DAC of DRoF is not needed at the remote unit, since the communication signal is recovered only by a band-pass filter [24]. This results in a much simplified remote unit, similar to ARoF. Overall, the SDoF provides the linearity of DRoF communication link, while maintaining low-cost and low-complexity remote units similar to ARoF.

It is worth to mention that, SDoF is enabled by the fact that digital signal processing (DSP) units and serial clock rates now are into the microwave regime. Without these developments, it would not be possible to consider SDoF for RF communication. Furthermore, the demands for high capacity interconnects in data centers is driving the development of binary transceivers and optical interconnects with higher and higher clock rates. SDoF benefits from these developments, since it can employ binary, digital communication links.

2.1   System Architecture

In Fig. 2.1, a general block diagram of a two-level, band-pass SDoF link is presented [23, 24]. As illustrated there, SDoF systems consist of three main blocks: a central unit, an optical communication link, and a remote unit. Starting at the central unit, a band-pass communication signal is modulated to a binary signal by a band-pass sigma-delta modulator. Then, the binary signal is converted to optical domain with an optical source, typically a laser. At the far end of the optical fiber, the electrical signal is recovered with a photo receiver. Thereafter, the quantization noise of SDM is suppressed by a band-pass filter to recover the up-converted, analog RF-signal, before the RF amplification, see Fig. 2.1. Finally, the analog signal is transmitted by an antenna. In the following sections, each block of SDoF link is discussed.
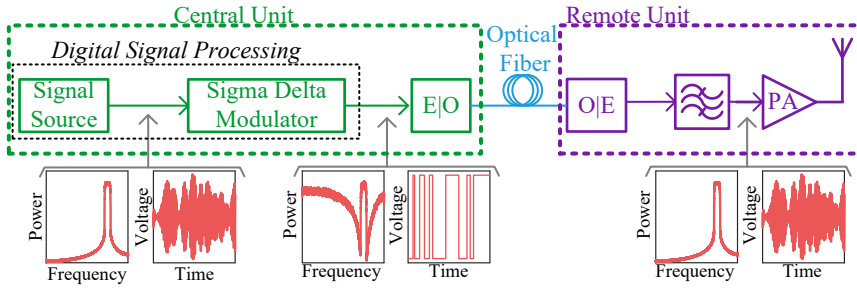
Figure 2.1: General structure of band-pass sigma-delta-over-fiber link including the spectra and waveforms. The recovered signal after the bandpass filter is also presented.
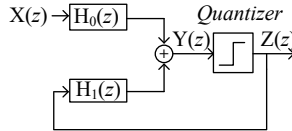
Figure 2.2: A z-domain model of sigma-delta modulation.

2.2 Central Unit

The central unit is the first block of a SDoF link, in which the digital signal processing and electrical to optical domain conversion is performed, see Fig. 2.1. The fundamental difference of the SDoF digital signal processing block compared to other RoF techniques, is using sigma-delta modulation to generate binary signals. Hence, the section starts with introducing the SDM, which is followed by a section about the electrical to optical conversion.

2.2.1 Sigma-Delta Modulation

Sigma-delta modulation is a technique where a waveform is quantized to a very low resolution signal with the help of oversampling and noise shaping. The quantization produces large, wideband noise-like distortion, referred as quantization noise. By oversampling, the quantization noise is spread over the frequency spectrum and by noise shaping, the quantization noise is shaped such that it is minimized in the band-of-interest. Overall, a very-high signal-to-noise-ratio (SNR) is achieved at the band-of-interest [25]. The in-band quantization noise is determined by the order of the SDM and the oversampling ratio (OSR) [25]. OSR is defined as the ratio of SDM sampling rate to Nyquist rate of the signal:

$$\text{OSR} = \frac{f_s}{2\text{BW}}, \tag{2.1}$$

where BW represents the bandwidth of the modulated RF signal.

A sigma-delta modulator can be modelled as shown in Fig. 2.2. The output of the loop-filter in (z)-domain is:

$$\text{Y}(z) = \text{H}_0(z)\text{X}(z) + \text{H}_1(z)\text{Z}(z). \tag{2.2}$$

The quantization can be represented as an addititive error signal source [26].
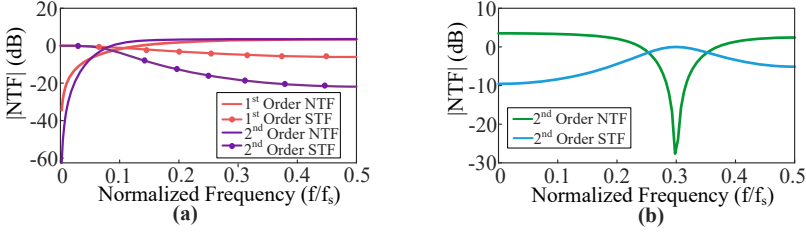
Figure 2.3: (a) Signal and noise transfer function magnitude of first and second order low-pass sigma-delta modulation. (b) Signal and noise transfer function magnitude of second order band-pass sigma-delta modulation.

The output of the modulator becomes:

$$Z(z) = Y(z) + E(z), \tag{2.3}$$

where $E(z)$ represents the white quantization noise, i.e. error signal. Using these two equations the output of the quantizer, $Z(z)$, can be re-written as:

$$Z(z) = \frac{H_0(z)}{1 - H_1(z)} X(z) + \frac{1}{1 - H_1(z)} E(z). \tag{2.4}$$

The transfer function of the modulator when the quantizer noise is neglected is denoted as signal transfer function (STF) and is equal to:

$$STF(z) = \frac{H_0(z)}{1 - H_1(z)}. \tag{2.5}$$

Similarly, the transfer function when the input is neglected, the noise transfer function (NTF), is:

$$NTF(z) = \frac{1}{1 - H_1(z)}. \tag{2.6}$$

Equation (2.6) suggests that, in order to minimize the quantization noise at a certain frequency range, $H_1(z)$ must be large at that frequency range. Furthermore, $H_0(z)$ must also be large at the same frequency in order to have a STF that is close to or larger than unity, see (2.5). The SD-moulator operating principle can only be represented by the STF and the NTF. By choosing appropriate loop filter transfer functions, $H_0(z)$ and $H_1(z)$, the quantization noise can be minimized at and around any frequency, while preserving the input signal quality. In this way, a high SNR will be achieved at the band of interest.

NTF and STF of first and second order low-pass and second order band-pass SDM are presented in Fig. 2.3 (a) and Fig. 2.3 (b), respectively. The minimized quantization noise and the unity STF at the band-of-interest is clearly visible. As mentioned previously, the in-band quantization noise can be decreased by increasing the order of SDM. This is also illustrated in the same figure. However, higher order SDM can result in unstable SDMs. Stability of a SDM depends on the maximum out of band gain, which is determined by the NTF(z) and the input signal magnitude range. There are no proven methods to assure the stability of SDMs. The most common criterion is given by Lee's Rule [27, 28]. According to that rule, a SDM is likely to be stable if

the maximum gain of NTF(z) over all frequencies is smaller than 1.5. However, this is more like a guide than a proven rule, since it does not consider the input range and there are some examples of stable SDM with a maximum gain larger than 1.5 [25].

2.2.2 Optical Source

After the sigma-delta modulation, the digital signal is transmitted to an optical source with a binary transmitter, e.g. FPGA. The electrical to optical conversion can be performed with many different types of lasers and optical modulators: single-mode laser diode [29], mach-zender modulator [30], vertical-cavity surface-emitting-laser (VCSEL) [31], electro-absorption modulator (EAM) [32]. Moreover, two-level SDoF communication links can also utilize standardized optical interconnects for datacom centers [33, 34]. Different types of small form-factor pluggable (SFP, SFP+, XFP, QSFP, QSFP+, QSFP28) and C-form-factor pluggable (CFP) transceivers are some of the most common ones.

2.3 Optical Fiber and Remote Unit

The central and the remote unit is connected to each other with an optical fiber, see Fig. 2.1. The optical fiber selection highly depends on the optical link distance. In general, single-mode-fibers are employed in SDoF communication links longer than few kilometers, for example, 25 km [35], 80 km [36] , whereas multi-mode-fibers are more common in shorter distances, 200 m [24].

The remote unit is responsible from electrical signal recovery, i.e. optical to electrical conversion, filtering the out-of band quantization noise, amplification of the signal and finally the transmission of the signal by an antenna. The optical conversion is performed either by a photo-diode [29] or with an optical interconnect transceiver as mentioned previously.

2.4 Discussion

Sigma-delta-over-fiber is not only limited to band-pass sigma-delta modulation and the presented structure. In the following sections, first, different implementations, and, then, the potential and limitations of SDoF communication technique are discussed.

2.4.1 Alternative Implementations

Low-pass sigma-delta modulation can be implemented to form SDoF communication links. The main difference between low-pass SDoF and band-pass SDoF is the up-conversion stage, see Fig. 2.4. Other than the up-conversion stage, the rest of the structure is highly similar to BP-SDoF. In BP-SDoF, the up-conversion is performed before the SDM in digital domain. However, in LP-SDoF, the up-conversion is performed after the SDM in digital domain, which requires extra measures, Fig. 2.4. For example, in [33,34,37,38] a parallel processing, time-interleaved method is implemented by employing multiplexers.
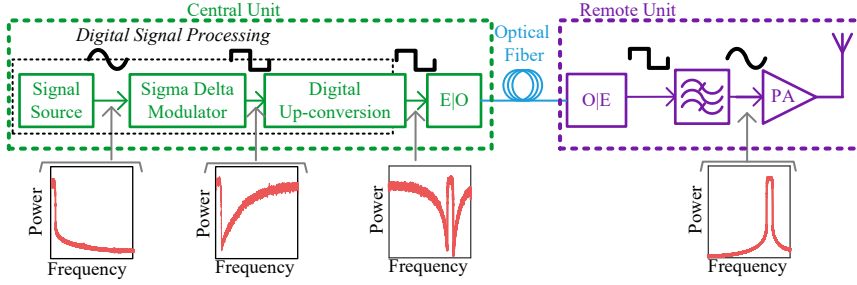
Figure 2.4: A general block diagram of low-pass sigma-delta-over-fiber communication link, including the frequency spectra at each step.

The up-conversion is typically performed by a 4×1 multiplexer operating at $f_m = 4f_c$. The low-pass sigma-delta modulated I, Q and their negative copies -I, -Q are transmitted in the presented order resulting in a carrier frequency $f_c = f_m/4$. As illustrated in Fig. 2.4, the quantization noise of the SDM RF-signal is suppressed at the remote unit by a band-pass filter, similar to BP-SDoF.

A more unorthodox method is presented in [30] to employ a carrier frequency $f_c = 60$ GHz. The low-pass sigma-delta modulated I-Q signal is first up-converted to 3.2 GHz by a multiplexer operating at 12.8 Gbps, as the method previously mentioned. Then, by using optical heterodyning, the carrier frequency is shifted to 60 GHz in optical domain.

In [29], a LP-SDM signal centered at 10 MHz is transmitted to the remote unit. The signal is first band-pass filtered to attenuate the quantization noise, then it is up-converted by a conventional analog mixer and local-oscillator stage. Compared to the previous digital-up conversion systems, the carrier frequency selection is less-limited. However, this method suffers from increased remote unit complexity compared to all the other mentioned methods.

In summary, low-pass SDM decreases the sampling requirements of the processor at the center unit, to the cost of limited range of center frequency.

2.4.2 Potential and Limitations

One of the major advantages of SDoF is that the up-conversion is performed in digital domain at the central unit. First of all, this decreases the cost, complexity and the package size of the remote unit by eliminating the traditional analog mixer and local oscillator stages. Furthermore, this facilitates fully synchronous communication links for systems that require phase coherent transmission from physically separated remote units. This will be further discussed in the following chapter.

In general, SDoF communication links are considered for downlink of a network cell. Forming the up-link with SDoF is not as appealing due to the required digital signal processing and the desire of keeping the remote unit simple. When SDoF is implemented for downlink communication, conventional ARoF can be employed at the up-link. This would require an additional optical source and a low-noise amplifier (LNA) at the remote unit. The optical to electrical conversion can simply be done by a photo-receiver at the central

unit. The main advantage of such implementation is the fact that, it does not require any mixers and local-oscillator stage at the remote unit for the up-link, which maintains the low-complexity. However, as mentioned previously, ARoF is sensitive to the non-linear distortion and limited by low-dynamic range.

SDoF provides flexibility in terms of the carrier frequency and symbol-rate. Let us consider a SDoF communication system with a carrier frequency of 1.5 GHz and operating at 5 Gbps sigma-delta sampling rate. The remote unit consists of, a band-pass filter centered at 1.5 GHz with a bandwidth matched to the RF-signal and a power amplifier (PA) with a fractional bandwidth of 97% at 2 GHz [39]. The Nyquist sampling theorem tells that, any center frequency up to 2.5 GHz can be employed with 5 Gbps sigma-delta sampling rate. The carrier frequency can be shifted to any frequency in the given range, just by replacing the band-pass filter and re-programming the sigma-delta modulator. Furthermore, the symbol-rate can also be changed in a similar way as long as the quantization noise does not become the limitation. The system can therefore be easily reconfigured in a cost efficient way.

SDoF is not limited to binary communication, since the SDM can generate signals with discrete levels more than one. However, all these developments make binary SDoF more appealing. Thus, the work presented in this thesis focuses on two-level, i.e. binary, SDoF communication links.

Chapter 3

Low-complexity Distributed MIMO Testbed

Multiple-input-multiple-output (MIMO) is a widely accepted technique to increase capacity, efficiency and reliability of a communication system based on channel diversity [40]. MIMO is a key enabling technology in previous (3G-HSPA+) [41], current (4G-LTE) [42] and emerging mobile communication systems (5G) [43]. A conventional system, which has closely located transmitter antenna elements is called co-located MIMO, whereas a distributed-MIMO system is formed by physically separated antenna units/access points (AP), see Fig. 3.1. Distributing the APs has many advantages but also several challenges. SDoF is a very promising technique as a facilitator of low-cost, low-complexity distributed MIMO systems.

In this chapter the different D-MIMO testbeds is first reviewed. Then, the proposed D-MIMO testbed based on SDoF in [Paper A] is described. Finally, the results of co-located- and distributed-MIMO measurements from [Paper B] are discussed in order to evaluate the potential and the performance of D-MIMO communication systems.

3.1 Distributed MIMO

A MIMO base-station, which has many closely located transmitter antennas can lead to highly correlated channels [44]. In such scenario where different channels are highly correlated, the capacity reduces significantly [45], which yields to poor reliability and reduced coverage. An alternative method to decrease the correlation and increase the system capacity, is distributing the transmit antennas, access points. In other words, forming a distributed MIMO system [46–52].

D-MIMO communication is a very promising technique to mitigate the high correlation related problems of conventional MIMO systems. However, there are many challenges that needs to be addressed when it comes to the practical realization. One of the key challenges is the RF-phase synchronization of physically distributed access points. Regardless of the distance between transmission antennas, any MIMO system requires accurate phase synchronization between
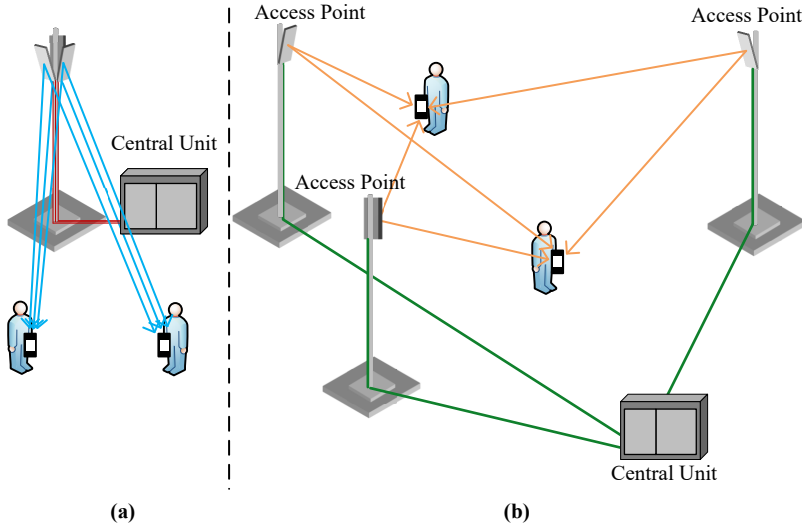
Figure 3.1: Illustration of downlink communication of conventional co-located MIMO (a) and distributed MIMO (b) system.

antennas/APs to perform MIMO techniques such as beamforming, interference nulling, etc. [53].

Fig. 3.1 (a) shows a simplified block diagram of the downlink of a multi-user MIMO (MU-MIMO) communication system with three base-station antennas serving two users. In a nutshell, MU-MIMO is a MIMO technique where the transmitter with multiple antennas serves multiple users with one or more receiver antennas. In Fig. 3.1 (a), the RF signals are transported from the base-station to the antennas at the base-station tower. Signals for different antennas are up-converted with a shared local-oscillator (LO) and mixer at the base-station providing a phase synchronous transmission. The main challenge of forming a distributed MIMO system is to maintain accurate phase synchronization between the spatially distributed APs. In Fig. 3.1 (b), an example of a D-MIMO transmitter is shown. If the baseband data provided by the central unit is up-converted at each antenna tower with individual LOs and mixers, the individual LOs of each access point will induce a different phase shift, destroying the phase alignment performed by the central unit for any joint transmission. On the other hand, transmitting up-converted RF-signals at the central unit via coaxial cables or wave-guides is not a solution due to the high attenuation levels and high cost. In conclusion, accurate RF-phase synchronization of APs is a fundamental challenge in D-MIMO systems due to the large distance between them, requiring additional measures compared to conventional, co-located systems, see Fig 3.1.

3.2   Distributed MIMO Testbeds

In reality, the limitations of distributed MIMO are not well understood due to the challenges of realizing such systems. Therefore, D-MIMO testbeds are needed to evaluate the practical limitations against theoretical predictions.
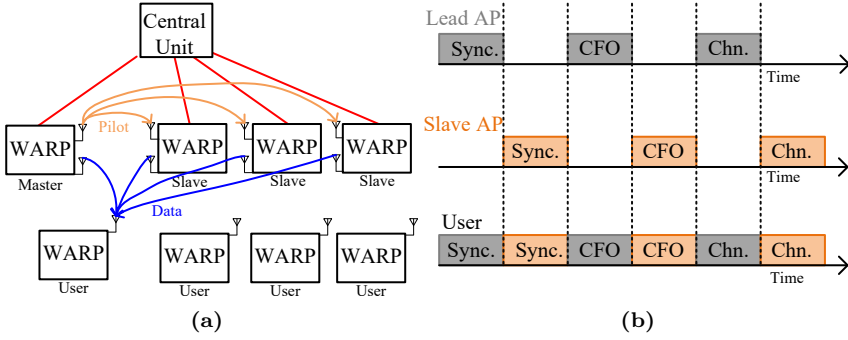
Figure 3.2: (a) The schematic of AirSync D-MIMO system, where one antenna of the slave access point (AP) continuously listens to the pilot transmission from the master AP and the other antenna transmits the information signals to the user. APs are formed by Wireless Open Access Research Platform (WARP). (b) The packet transmission sequence of MEGAMIMO D-MIMO system, symbols in grey are transmitted from the lead AP and symbols in orange are transmitted from the slave AP. Transmission of channel estimation symbols (Chn.) are repeated and interleaved from different APs.

Different solutions have been proposed to realize distributed MIMO systems with synchronized APs [53–57]. These D-MIMO implementations are designed for real-time communication systems and they are costly and complicated when it comes to the experimental studies of D-MIMO. Hence, there is also a need for low-cost, low-complexity platforms aimed for initial and fundamental D-MIMO studies and experiments at an early stage. In [Paper A], this problem is addressed and a fully synchronized D-MIMO testbed for MIMO downlink communication, integrated with high-speed SDoF is proposed. It is worth to mention that the proposed testbed is aimed for conducting measurements and analysis of distributed MIMO communication systems in real environments. Therefore, the testbed consists of a SDoF based D-MIMO downlink and an ideal up-link formed by an Ethernet connection.

In general, the D-MIMO testbeds provide RF-phase synchronous access points either by wireless or by hardware synchronization. Both of these synchronization methods have their own advantages and disadvantages in terms of: additional signal processing, access point complexity, the possible antenna deployment distance, etc. In the following sections these testbeds are reviewed in terms of their synchronization method and access point complexity.

3.2.1 AirSync

AirSync [53] was one of the first fully distributed real-time MIMO communication systems. It employs a wireless synchronization technique to achieve a phase coherent transmission from APs. In AirSync, all the APs are connected to a central unit, which is responsible for distribution of the baseband signals , see Fig. 3.2 (a). One of the APs in a cluster, i.e. network cell, is selected as master (reference) AP whereas all the others become slave APs. Every slave AP has two antennas: one dedicated antenna for the reception of the pilot signals transmitted by the master AP and one antenna for the actual information signal transmission. Every slave AP measures the instantaneous phase of the pilot

signals transmitted by the master AP and compensates for it while transmitting the information signal from the second antenna. The synchronization pilot signals are placed outside the information signal bandwidth, which facilitates a simultaneous transmission and synchronization. The extensive signal processing performed at each AP requires powerful and complicated APs. In AirSync, the APs are formed by wireless open access research platform (WARP) radio units [58], which consists of FPGAs, RF front-ends, clock boards, etc. Moreover, the pilot transmission from the master AP to the slave APs require them to be within communication range, which can limit the maximum deployment area of the APs. On the other hand, the authors suggest a relay communication method, in which every AP forwards the received pilot signals to the next AP, as a solution for this problem. As a summary, AirSync successfully demonstrates synchronized D-MIMO communication through wireless synchronization to the cost of complex signal processing, costly and complicated APs and limited distance for AP deployment.

3.2.2   MegaMIMO and MegaMIMO 2.0

MegaMIMO [54] and MegaMIMO 2.0 [57] also provide phase coherent D-MIMO communication with wireless synchronization. Similar to AirSync, these testbeds also divide the APs in two categories: lead AP and slave APs. The transmission sequence starts with a synchronization header transmitted by the lead AP, see Fig. 3.2 (b). Each slave AP then calculates the phase drift of its LO from the lead APs LO. The predicted phase difference is used later for compensation to achieve coherent data transmission. After synchronization header transmission, lead and slave APs transmit channel measurement blocks one at a time. In this way, the APs do not interfere with each other and interleaving packets provide a close approximation to simultaneous measurement of the channels from all the APs to a client. Finally, the APs use the estimated relative phase offset and the channel state information for a joint data transmission to the clients. The synchronization and channel measurements are repeated according to the coherence time of the channel.

The MegaMIMO system is upgraded with a distributed power control and full-fledged real-time 802.11 PHY in MegaMIMO 2.0. Similar to AirSync, both the MegaMIMO systems require complex and expensive APs in order to perform all the necessary computations required for joint transmission. In MegaMIMO, the APs are formed by USRP2 boards and RFX2400 daughterboards [59]. In MegaMIMO 2.0, the APs are realized by Zedboard [60] connected to an Analog Device FMCOMMS2 transceiver card [61].

3.2.3   Vidyut

A rather different approach than the previous testbeds is used in the Vidyut D-MIMO testbed [56]. In Vidyut, all the APs and the central server are connected to the electrical power lines of the building complex, see Fig. 3.3 (a). These electrical power lines are used to transmit a 10-MHz reference clock from the central server to the APs. At each AP, the reference clock is first bandpass filtered and then fed to the PLL of the clock distribution circuit, see Fig. 3.3 (b). The clock distribution circuit has three outputs: one is used as
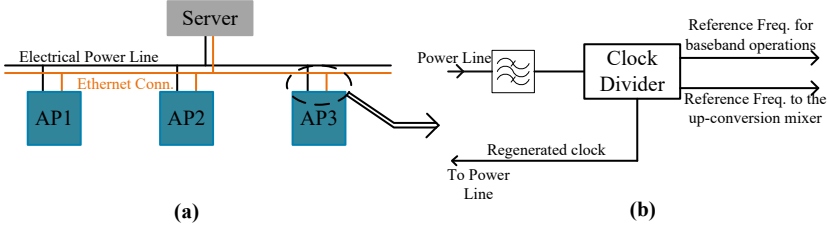
Figure 3.3: (a) Vidyut D-MIMO testbed connection and (b) clock distribution diagram. Three outputs of PLL based clock divider is also presented.

clock for baseband operations, the second output is fed to the up-conversion mixers and the third output is fed back to the power lines to overcome the attenuation of the power distribution network. At each AP there is also an isolation transformer to protect the circuit from the high voltage of the electrical power lines. For the transmission of baseband data, another link between the central server and the APs is established with an ethernet connection. The APs of the Vidyut are formed by NI-5791 [62] radio front-ends, which are also equipped by a PLL based clock distribution core AD9511. Compared to previously mentioned testbeds, Vidyut requires less complex and cheaper APs. However the main drawback of Vidyut is that the system depends on the established electrical power lines.

3.2.4 Zinwave and PCell

There are also commercial products such as Zinwave [63] and Pcell [64] for realizing D-MIMO communication systems. Generally, these products are closed systems and developed to meet a specific standard, for example PCell is developed for LTE communication standards. Thus, these products are not suitable for theoretical studies of new D-MIMO communication concepts beyond currently existing standards and use cases.

3.3 Sigma-Delta-over-Fiber based D-MIMO

There are multiple testbeds, which can successfully demonstrate D-MIMO communication. However, these testbeds are aimed for real-time communication systems and either they are costly for experimental D-MIMO studies or they are not completely flexible in terms of carrier frequency, symbol rate, modulation order, number of transmission channels, etc. As shown in the previous section, one of the main hurdles of realizing a D-MIMO system is providing RF-phase synchronous APs for a joint transmission.

SDoF communication technique enables spatially distributed, full synchronized channels with very low-complexity APs, see Chapter 2. In a nutshell, SDoF employs sigma-delta modulation to modulate an information carrying RF-signal to a bi-level (one-bit) digital signal by oversampling and noise shaping. Digital domain up-conversion performed at the central unit decreases the cost, complexity and size of the AP since the traditional mixer and local oscillator stages are not required any more. More importantly, it enables coherent signal
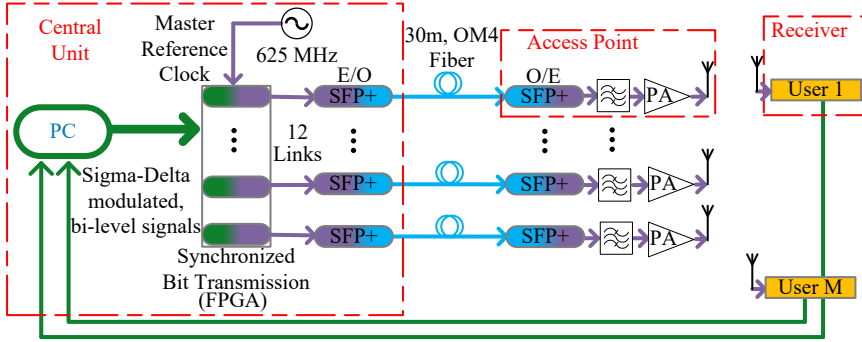
Figure 3.4: The schematic of the presented sigma-delta-over-fiber based D-MIMO testbed. Twelve sigma-delta modulated bit-streams are created in MATLAB and uploaded to the FPGA. The output of twelve multi-gigabit transmitters of the FPGA are converted to the optical domain with SFP+ modules followed by 30m, OM4, multi-mode fiber (MMF). The received signal at the access points the electrical signal is recreated with SFP+ modules and then the RF-signal is recovered with bandpass filters. Finally, the recovered RF-signal is amplified with PA and transmitted with a patch antenna. The receiver/client is formed with an signal analyser (Agilent N9030A) controlled by the same PC.

transmission from physically distributed APs, since all the signals are generated from the same digital clock at the central unit. Furthermore, the bi-level nature of SDoF communication facilitates the use of low-cost, low-dynamic range optical components produced for high speed datacom applications. The following section presents the implementation of a SDoF based testbed for D-MIMO experiments.

3.3.1   Testbed

The testbed hardware can be divided into two parts: The central unit, where all the signal processing, signal generation and electrical to optical conversion is done, and the AP at the far end of the optical link, where the optical to electrical conversion, bandpass filtering, amplification and antenna transmission is performed.

Fig. 3.4, shows the schematic of the testbed with twelve fully coherent transmission channels. The testbed is designed for C- and D-MIMO experiments with the main focus of joint signal transmission from spatially distributed APs. Therefore, during the measurements an ideal up-link is assumed and formed by an Ethernet connection. The user equipment is represented by a receiver instrument (Agilent N9030A), which is controlled by the same computer used for offline communication signal processing and control of the central unit.

Central Unit

The central unit is realized by an FPGA development board (Transceiver Signal Integrity Development Kit, Stratix V GT Edition). The FPGA board has 28 × 12.5 Gbps and 4 × 28 Gbps high speed transceivers. Out of these 28 transceivers, 12 of them are used to implement the SDoF links.

To synchronize all the communication links for a coherent transmission, a 625-MHz external master clock is connected to the FPGA development board.
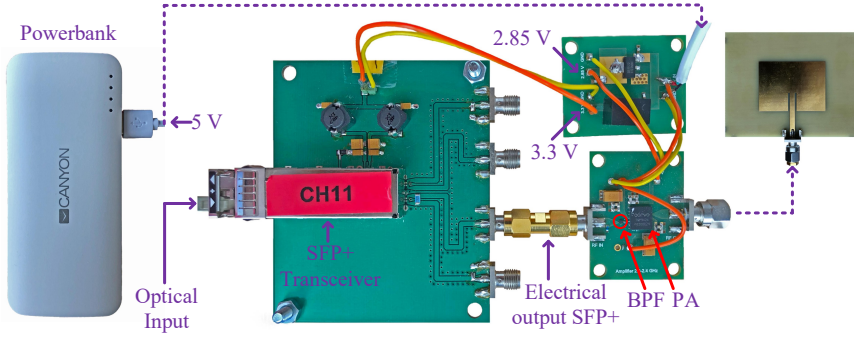
Figure 3.5: Photo of one of the twelve identical access points. First, the received optical signal is converted the electrical domain by using an SFP+ transceiver. Thereafter, the signal is bandpass filtered and amplified before the transmission with a patch antenna. A powerbank with 5 V output in combination with two different voltage regulators (2.85 V and 3.3 V) is used as a power source.

Two PLLs, each serving six channels, are synchronized to the same master clock, which provides twelve RF-phase coherent transmitter channels.

Twelve, up-converted and oversampled RF signals are sigma-delta modulated (2nd order) with MATLAB toolbox [25] and uploaded to twelve random-access-memories (RAM) of the FPGA board. The FPGA board continuously reads the data from the RAMs and transmits them to small form-factor pluggable transceivers (SFP+, Avago AFBR-709SMZ). The optical signals, converted by the SFP+ transceiver modules, are transmitted to another SFP+ module at the access point through a 30m, OM4 multi-mode fiber (MMF). The SFP+ transceivers support maximum transmission rate of 10 Gbps with a maximum distance of 300 meters. In other words, the current testbed configuration enables approximately 600m coverage.

It is also possible to implement sigma-delta modulation at the FPGA [33, 65–69] instead of offline processing in MATLAB. This was not implemented in the proposed testbed, since focus of the testbed is to provide a low-complexity platform for D-MIMO evaluation experiments rather than a real-time communication system.

Access Point

At the access point, first the received optical signal is converted to electrical domain by an SFP+ transceiver, see Fig. 3.5. Thereafter, the original RF-signal is recovered by a bulk-acoustive wave (BAW) commercial bandpass filter. After the bandpass filter, the signal is amplified with a commercial power amplifier (PA, Qorvo TQP9424), which provides 36 dB gain at the band of interest. Finally, the signal is transmitted by microstrip patch antenna.

To provide flexible deployment of the APs, they are equipped with a DC-power source (USB Powerbank, 5 V, 13000 mAh) and mounted into a plastic box. The required supply voltage levels at the APs are supplied from two different voltage regulators (2.85 V and 3.3 V). In this way, more than 10 hours of operating time is achieved without any need of external power supply.

3.3.2   Flexibility

Integrating the SDoF technique to distributed MIMO systems not only provides RF-phase synchronous access points, but also enables flexibility throughout the D-MIMO communication system in terms of the hardware, signal processing algorithms and signal parameters. The digital up-conversion at the central unit enables the carrier frequency to be changed only by replacing the bandpass filter and changing sigma-delta modulation parameters. The implemented FPGA and SFP+ are able to support up to 10 Gbps and 12.5 Gbps bitrates, respectively, enabling carrier frequencies up to 5 GHz. The number of fully synchronized channels can be increased up to 28 with the current FPGA platform. Moreover, the implemented FPGA supports four, synchronized channels with 28 Gbps maximum bit-rate. Simply by replacing the SFP+ transceivers with QSFP+ modules, which support up to 40 Gbps optical communication, these four channels of the FPGA can be used. This upgrade enables carrier frequencies up to 14 GHz at four coherent transmission channels. The number of channels, maximum carrier frequency and symbol rate can be easily increased as more advanced FPGAs are available. For example, one of the newer FPGAs from Intel (Stratix 10 TX), supports up to 120 GXE transceivers, each with a maximum bit-rate of 30 Gbps. The flexibility of the current testbed in terms of the carrier frequency and symbol-rate is demonstrated in the following section.

3.3.3   Evaluation of the Testbed

The implemented testbed is evaluated in various ways before the D-MIMO communication experiments. First, the carrier frequency and the modulation flexibility, then the synchronization of different transmission channels and finally the robustness of the channel estimation algorithm is assessed.

Carrier Frequency and Symbol-rate Flexibility

As mentioned previously, one of the major advantages of SDoF based D-MIMO is its flexibility and this section demonstrates it in terms of the symbol-rate and carrier frequency.

Performing the up-conversion in digital domain and the constant quantization noise of SDM with respect to carrier frequency [25], makes it possible to realize any carrier frequency in the first Nyquist zone only by replacing the bandpass filter at the AP and changing the sigma-delta modulation parameters. To verify the constant quantization noise of SDM with respect to carrier frequency, signals centered at different center frequencies are transmitted and the EVM of the transmitted symbols are calculated. During the measurements a symbol-rate of 2.5 Msym/s is used and the receiver instrument is connected to the output of the FPGA. Furthermore, the same measurements are performed at the electrical output of the SFP+ at the access point. Output of the bandpass filter is not measured since it has a narrow pass-band and designed for a single test carrier frequency.

The EVM of the transmitted symbols and the output in-band power of the FPGA with respect to carrier frequency is presented in Fig. 3.6 (a). Despite the theory [25], the EVM of the transmitted symbols increases versus carrier frequency. This can be explained by the decreasing output power of the FPGA
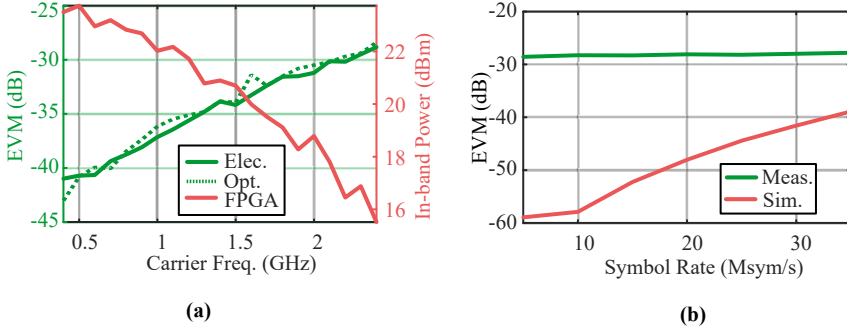
Figure 3.6: (a) Error-vector-magnitude of transmitted symbols measured at the output of the FPGA (Elec.) and at the electrical output of the SFP+ located at the access point (Opt.). The in-band output power of the FPGA with respect to frequency is presented on the right axis. (b) Measured error-vector-magnitude at the output of the SFP+ (Meas.) compared with simulated (Sim.) for different symbol-rates.

for higher carrier frequencies. Lower output power with a constant FPGA noise power leads to SNR degradation, which results in higher EVM. Moreover, the EVM measured at the output of the SFP+ shows that the signal quality, i.e. SNR, is not affected by the optical link. Indicating the fact that optical interface has a lower noise level than the FPGA, thus the EVM is preserved throughout the optical link. In conclusion, the FPGA frequency response limits the performance. Nevertheless, even for the highest tested frequency EVM of the transmitted symbols is $\sim$ -28 dB.

Another flexibility of the testbed is demonstrated by transmitting signals with different symbol rates, centered at 2.365 GHz. The transmitted signals are acquired at the electrical output of the SFP+. Fig.3.6 shows the measured (Meas.) and simulated (Sim.) EVM for different symbol rates. The EVM of the simulated symbols increases for higher symbol rates due to the increased in-band quantization noise [25]. On the other hand, large oversampling ratio, i.e. very low in-band quantization noise, and the noise power level of the FPGA makes this invisible in the measurements. The bandwidth of the receiver instrument limits the maximum transmitted symbol-rate to 35-Msym/s. However, even with 35-Msym/s the quantization noise is still lower than the FPGA noise level, see Fig.3.6. The simulations show that the symbol rate resulting in -28.5 dB EVM is 65-Msym/s. Hence, the testbed can preserve transmit signal quality up to 65-Msym/s. In order to employ higher symbol rates than 65 Msym/s with compromising the performance of the communication link the quantization noise of the SDM has to be decreased. This can be performed by increasing the oversampling ratio, see Chapter 2.

Phase Synchronization and Channel Estimation Performance

The phase synchronization of different transmission channels of the testbed is examined by transmitting the same signal simultaneously from two different channels. The signals are captured by a multi-channel oscilloscope (Agilent, Infiinum 5854A DSO) and processed in MATLAB. The phase difference between the symbols are calculated and presented in Fig. 3.7 (a). The standard
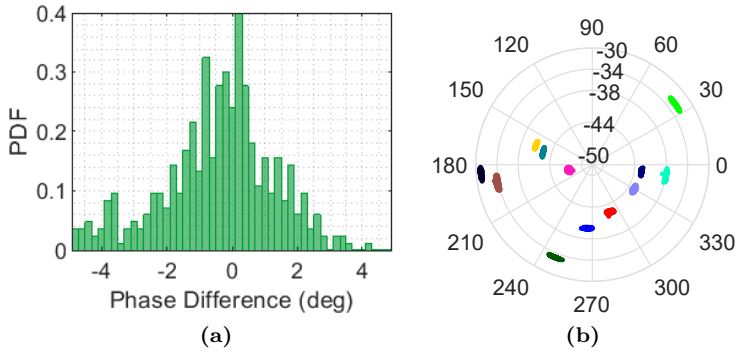
Figure 3.7: (a) Probability density function (PDF) of phase difference between two randomly picked transmission channels of the testbed, measured at the output of the power amplifier. (b) The 600 channel estimations measured at the same position. Each color represents each complex element of the channel matrix, H and the radius represents the received power in dBm. The small spread of the 600 channel estimations indicates that the transmission links of the testbed are well synchronized.

deviation of the phase difference is 2.1°, indicating an accurate, tight phase synchronization between different transmission channels.

After the verification of the phase synchronization, the performance of the channel estimation algorithm is evaluated with all the twelve channels. The APs are deployed in the measurement room as shown in Fig. 3.8. Without moving the receiver, 600 channel estimation measurements are performed and the channel is estimated for each measurement. Fig. 3.7 (b) shows the estimated channel coefficients of the 600 measurements. The standard deviation of the estimated channel coefficients phase is 2.7° and amplitude is 0.03 dB, which again shows that the different transmission channels of the testbed are well synchronized. This also verifies that the implemented channel estimation algorithm is performing as expected. Even so, to investigate the effect of the channel estimation uncertainty, 600 new measurements are taken. One of the 600 previous channel measurements is used as precoder and 600 new independent signals are transmitted. The results show that the uncertainty in channel estimation, does not have any significant effect on the communication quality.

In conclusion, the results of the investigations presented in this section have shown that the proposed testbed can provide multiple, very well synchronized data channels suitable for D-MIMO experiments.

3.4 Experiments

The main aim of the testbed is to provide a low-complexity, low-cost fully synchronized, multi-channel platform for D-MIMO experiments. After all the verifications mentioned previously, the testbed is used in various measurements to compare D-MIMO and co-located MIMO. In this section, the results of the comparison measurements from paper [Paper B] is presented.

3.4.1 Measurement Method

All the experiments are performed in a laboratory providing a rich scatterer environment with tables, measurement racks, cabinets, etc, see Fig. 3.8. Same signal analyser used for verification measurements is formed the receiver with a mono-polo WI-FI antenna. Each access point is mounted to the walls as showed in Fig. 3.8 approximately two meters above the floor. All measurements are performed with a 16-QAM, 5-Msym/s RF-signal centered at 2.365 GHz and modulated with 2nd order bandpass sigma-delta modulator.

Measurements are conducted in thirty-one different locations and at each location first single user, then multi-user MIMO communication experiments are performed. Each measurement starts with a channel estimation phase to calculate the channel matrix. After the estimation of the channel matrix, first single user measurement with beamforming precoding, then two and three user measurements, i.e. MU-MIMO, with ZFBF precoding are performed. During two and three user measurements, one of the clients are always formed by the receiver at the current location and the other clients are randomly picked from the previous measurement locations. This enables the receiver instrument to always move to next location without returning to a previous measurement location. In this way the measurement consistency and speed increases significantly. It is worth to mention that; this procedure is possible because the ZFBF algorithm is fair to each user in terms of the transmitted power and the interference. At every location, up to 8 different two user and three user measurements are performed, resulting in 31, 212, 212 unique 1-, 2-, 3-user measurements, respectively, for C- and D-MIMO.

3.4.2 Results

The co-located and distributed MIMO experiment results are compared in terms of the received power, received symbol EVM and inter-user interference.

Multiple-input-single-output

Fig. 3.8 shows the measurement lab and thirty one measurement locations used in the experiments. The received power of both C- and D-MISO is also presented. The distribution of the received power across the room is presented in Fig. 3.9. Both figures show that distributing the access points increases the coverage in the room, compare to co-located access points by increasing the received power. It is worth mentioning that, in certain receiver locations co-located MISO delivers higher power, especially when the receiver is in the line-of-sight of the closely located APs. However, in some locations the received power decreases significantly compared to D-MISO. Overall, D-MISO outperforms C-MISO by increasing the received power.

In Table. 3.1 the average EVM of the received symbols is presented for both C- and D-MISO. The similar EVM values despite the different average received power is mainly due to the linearity of the testbed, relatively small size of the measurement laboratory and the high sensitivity of the receiver instrument.
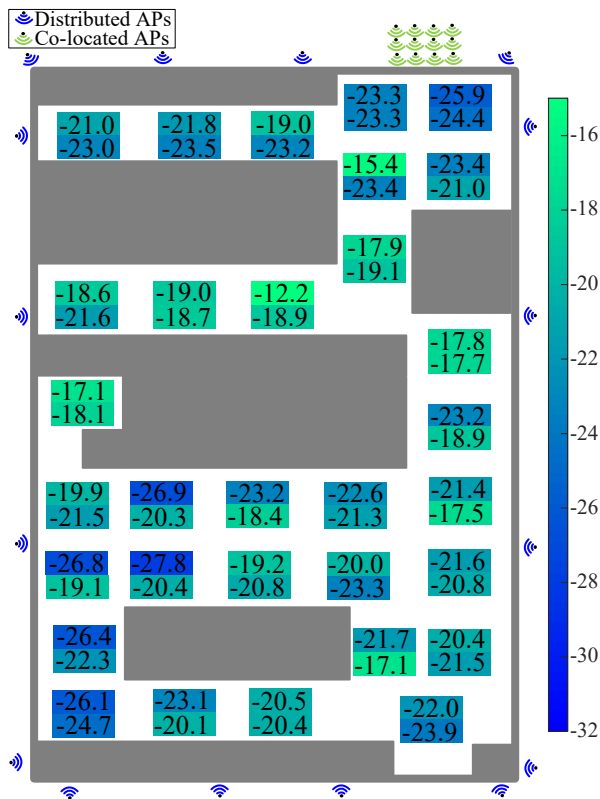
Figure 3.8: Measurement laboratory illustration showing the measurement locations and the received powers for single user experiments. At each box, bottom value and top value represents distributed and co-located access points, respectively.
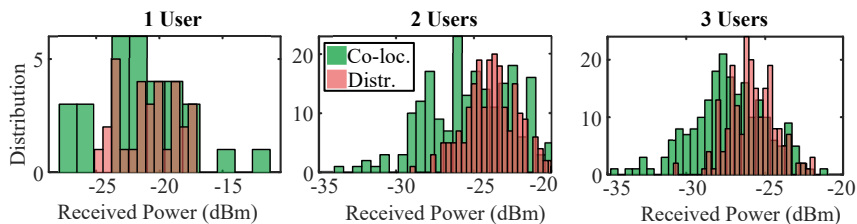
Figure 3.9: The distributions of the received power throughout the measurement laboratory for different number of users.

Table 3.1: AVERAGE ERROR-VECTOR-MAGNITUDE (EVM) AND SIGNAL-TO-INTERFERENCE RATIO (SIR) OF DIFFERENT NUMBER OF USERS FOR DISTRIBUTED AND CO-LOCATED MIMO.

	EVM (dB)		SIR (dB)	
	Distr.	Co-loc.	Distr.	Co-loc.
1-User	-28.4	-27.4	-	-
2-Users	-22.0	-20.4	23.2	22.8
3-Users	-18.7	-17.4	19.6	19.4

Multi-User Multiple-input-multiple-output

In Fig. 3.9 the received power distribution of all 212 measurements conducted with 2- and 3-users are presented for C- and D-MIMO. Similar to MISO case, distributed MU-MIMO delivers more uniform power levels compared to co-located MU-MIMO. The average EVM and signal-to-interference ratio (SIR) is presented in Table 3.1. The results show that distributing the APs can increase the EVM and SIR compared to C-MIMO. The main reason of EVM degradation when the number of users is increased, is the residuals of interference. Theoretically [70], ZFBF eliminates all the inter-user interference with a perfect CSI, however the imperfect channel estimation results in interference residuals, which explains the EVM degradation.

In [paper B] another MU-MIMO precoding technique, maximal-ratio-combining (MRC) [71] is implemented. MRC is a precoding technique, which maximizes the receiver power at each user without considering the inter-user interference. In general, ZFBF pre-coding is implemented if the communication system is interference limited while MRC is used for signal-to-noise ratio (SNR) limited scenarios. The experiments in [paper B], show that the communication system is highly interference limited and this is mainly due to the relatively small size of the measurement laboratory. Therefore, further experiments are not performed with MRC precoding.

3.5   Discussion

Distributing the access points is an alternative of conventional, co-located MIMO, which can improve the capacity, coverage and the reliability when the channels between the transmitter and receiver is highly correlated. However, the well-known theoretical advantages of D-MIMO can only be achieved with RF-phase synchronous access points. The proposed testbeds are implemented for real-time communication systems and they are costly and complicated. Thus, there is a need of a low-complexity, low-cost testbed aimed for performing experiments to analyse distributed MIMO communication in real environments.

In paper [Paper A] a novel solution is proposed to form a testbed for D-MIMO experiments enabled by employing sigma-delta-over-fiber. The testbed utilizes all-digital downlink transmission channels between the central unit and the access points and provide excellent RF phase coherence between the widely separated access points without additional hardware. The all-digital nature of the testbed makes it very flexible and future-proof, since it can be upgraded easily when new digital communication technologies such as FPGA, digital optical transceivers, etc, are available.

Chapter 4

Ultra-High Speed Sigma-Delta-over-Fiber

In the previous chapter, the potential and limitations of SDoF for multiple, phase coherent transmitters, i.e. distributed-MIMO, are investigated. It is shown that, tightly synchronized D-MIMO communication links can be formed with SDoF due to the digital up-conversion performed with a shared local-oscillator/clock at the central unit. The benefits of SDoF communication links are not only limited to MIMO systems. SDoF can be implemented to realize ultra-wide bandwidth, beyond 10 GHz, cost-efficient communication systems. Such communication links are achievable due to the two-level output of SDM, which facilitates to use low-dynamic range and low-cost optical sources such as vertical-cavity surface-emitting-lasers (VCSEL).

In this chapter, the limitations and potentials of ultra-high speed SDoF communication links are investigated with state-of-the-art VCSELs. A SDoF link is formed by different VCSELs and assessed with beyond 10 GHz signals. First, the effects of VCSEL characteristics on ultra-high speed SDoF communication links are examined [Paper C]. Thereafter, the potentials and limitations in terms of the data-rate and carrier frequency are investigated [Paper D].

4.1   Vertical-Cavity Surface-Emitting-Laser

VCSEL is a semiconductor laser diode, which was proposed in 1977 by professor K.Iga at Tokyo Institute of Technology [72]. In compare to conventional edge-emitting lasers, VCSELs have a light output perpendicular to its surface, see Fig. 4.1 (a). Even though VCSELs are mostly utilized in datacom centers as optical sources, they are used in many different applications from sensing to communication. Atomic clocks [73], laser printers [74], face identification of Apple devices [75], gas analysis [76] and optical computer mouse [77] are some of these applications.

The low manufacturing and packaging costs enabled by wafer-scale testing and screening are some of the major benefits of VCSELs [78]. Moreover, use of plastic coupling optics and large alignment tolerance to multi-mode-fibers (MMF) makes VCSELs even more popular. VCSELs also provide small
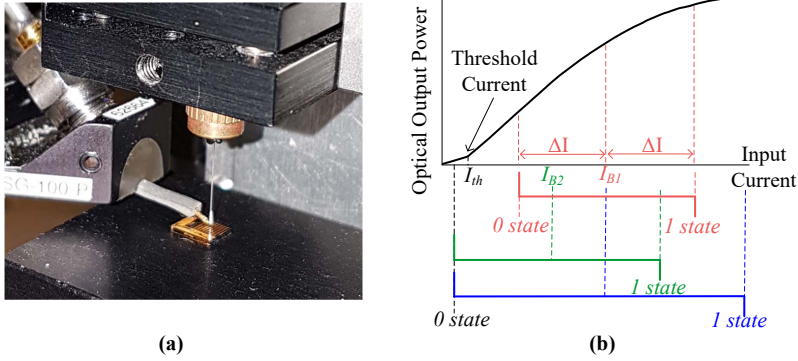
Figure 4.1: (a) A chip with multiple VCSELs on it and one of the VCSELs is coupled directly to optical fiber.(b)Illustration of three different modulation conditions for a VCSEL. I_{th} and I_{B} represents the threshold and bias current, respectively. The first condition (red curve) has bias current I_{B1} and both states are above threshold. The second condition (green curve) has the same modulation amplitude as the first condition but a smaller bias current, I_{B2}, resulting in subthreshold 0-state. The third condition (blue curve) has the same bias current with the first condition, I_{B1}, however with a larger modulation modulation amplitude then the first condition, which yields to subthreshold 0-state.

footprint required for low power consumption and high bandwidth density. Overall, these properties make VCSELs very good candidates as optical sources for ultra-high speed SDoF communication links.

4.1.1   Operational Considerations

One important fact to consider when using VCSELs, is avoiding subthreshold 0-state. In other words, turning-off the laser when '0' signal is transmitted. This is mainly due to the unwanted results of subthreshold 0-state such as turn-on delay and power overshoot. The consequences of both are explained further in the following section. In Fig. 4.1 (b) three different modulation conditions are illustrated. The red curve represents the case where subthreshold 0-state is avoided by using a certain modulation amplitude and bias current. In the case represented by the green curve, the same modulation amplitude is used with a lower bias current resulting in a subthreshold 0-state operation. The blue curve represents the case where the bias current is same with the operation represented by the red curve, however with a higher modulation amplitude, again resulting in a subthreshold 0-state. These three illustrations show that to avoid subthreshold 0-state operation, both the modulation amplitude and the bias current has to be chosen carefully.

Furthermore, choosing a correct bias current and input modulation is not only important for avoiding the subthreshold 0-state but also important for energy efficiency, lifespan, bandwidth (determined by the bias current), etc. For example, larger modulation amplitudes require higher bias currents in order to avoid threshold, which results in low energy efficiency and low potential lifespan of the VCSEL. All of these mentioned properties are highly effected by the VCSEL oxide aperture size as well.

These effects of the VCSEL characteristics and operating points are less-
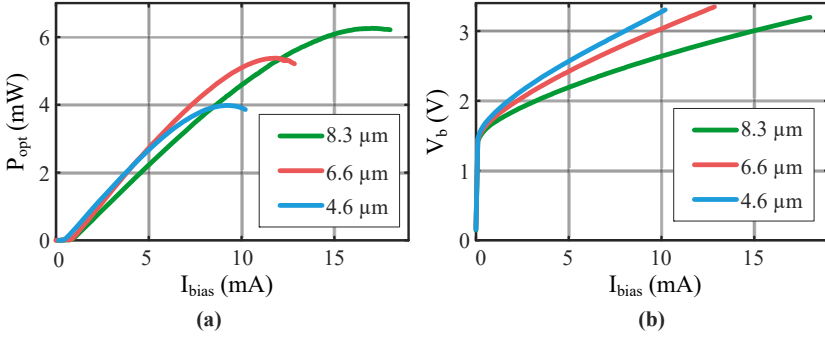
Figure 4.2: DC characteristics of each VCSEL. (a) Optical output power and (b) voltage drop with respect to bias current.

known for SDoF communication links especially for beyond 10 GHz systems. The following sections demonstrate the trade-offs between VCSEL characteristics and operating points, oxide aperture sizes.

4.2   Experimented VCSELs

For the evaluation experiments, the ultra-high-speed SDoF communication links are formed by three 850 nm state-of-the-art VCSELs. These VCSELs are GaAs-based and the design procedures are described in detail in [79]. The procedure that is explained in [79], enabled a 8 μm VCSEL to achieve a record high OOK data transmission rate of 55 Gbps over 50m of OM4-fiber without equalization electronics [80]. All the experiments are performed with VCSELs that are manufactured in Chalmers University of Technology with the same technology.

Fig. 4.2 shows the steady-state characteristics of the three VCSELs at room temperature. The left and right graphs present the optical output power (a) and the voltage drop (b) with respect to bias current, respectively. When three VCSELs are compared, VCSELs with larger oxide apertures have higher maximum output power, larger threshold current and a lower differential resistance.

Small-signal modulation response of each VCSEL is shown in Fig. 4.3. The highest 3-dB bandwidth of each VCSEL for the presented bias currents are ~24.5 GHz (at I_{bias}=8mA), 23.5 GHz (at I_{bias}=10mA) and 23.5 GHz (at I_{bias}=12mA) for the VCSELs with oxide aperture size of 4.6 μm, 6.6 μm and 8.3 μm, respectively.

4.3   Effects of VCSEL Characteristics

Optical interconnects based on directly modulated VCSELs and multi-mode-fibers (MMF) are today widely used in datacom applications [81]. Hence, the effects of VCSEL characteristics on optical datacom links are well-known. On the other hand, the effects are less-known for SDoF communication links.
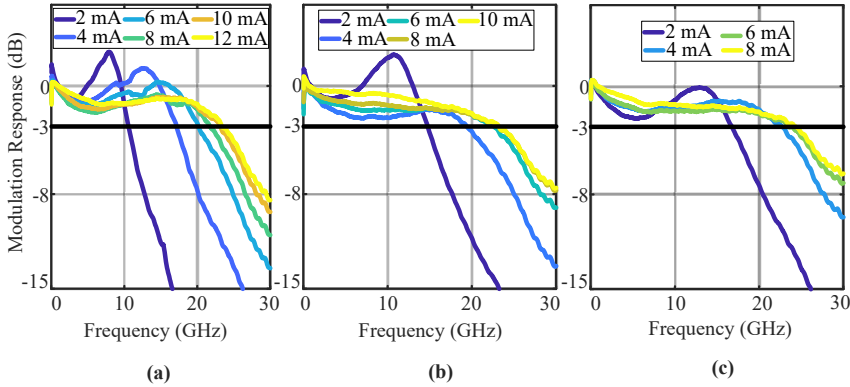
Figure 4.3: Small-signal modulation response (S21) for VCSELs with oxide aperture sizes of 8.3 μm (a), 6.6 μm (b) and 4.6 μm (c) with respect to bias current. The modulation response is normalized by dividing with its value at 1 GHz. 3-dB bandwidth of the VCSELs are also shown (black line) for each VCSEL.

One of the earlier SDoF studies [23], investigated the effects of VCSEL bias current and modulation amplitude on signal quality by employing a 1550-nm VCSEL as an optical source. However, the investigations was performed for signals with carrier frequencies up to 2.25 GHz. In paper [Paper C], the investigation is extended to carrier frequencies beyond 10 GHz. In addition, VCSELs with different oxide aperture sizes are evaluated. Three, state-of-the-art, 850-nm-wavelength VCSELs with oxide aperture sizes of 8.3, 6.6 and 4.6 μm are employed. Furthermore, various bias currents and input modulation voltages are also tested in order to discover the trade-offs between aperture size, bias current, modulation voltage and signal quality, energy efficiency, lifespan.

During the experiments a 64-QAM, 160 Msym/s RF-signal centered at 12 GHz and modulated by a 32 Gbps bandpass SDM (OSR = 100) is used as a reference signal.

4.3.1 Turn-on Delay and Power Overshoot

As mentioned previously, subthreshold 0-state leads to signal quality degradation due to power overshoot and turn-on delay. When the electrical input of the VCSEL suddenly changed to switch from 0-state to the 1-state (or vice versa), the optical output will reach to its new state undergoing damped relaxation oscillations [82]. This can result in power over- and under-shooting in the transient part of the output response. Furthermore, when the input current changes suddenly from 0- to 1-state, it takes a certain time for the laser to react, i.e. start lasing, which is called turn-on delay. The power overshoot and turn-on delay becomes stronger when the 0-state is below or close to the threshold, resulting in significant pulse distortion. To avoid such effects higher bias currents should be used, which leads to lower energy efficiency. Thus, there is a trade-off between pulse distortion and energy efficiency for the VCSELs.
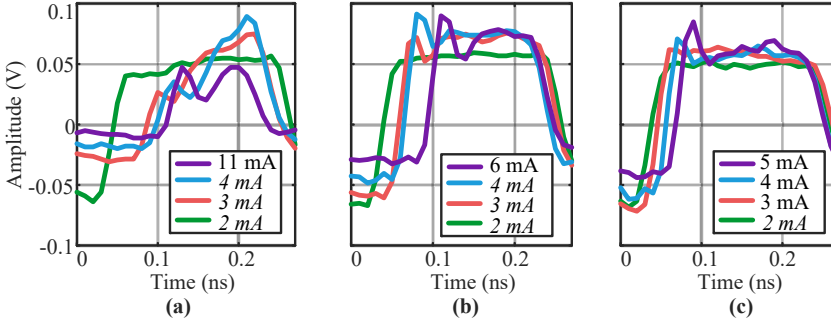
Figure 4.4: Time domain pulse response measured at the electrical output of the photoreceiver as a function of VCSEL bias current for the three employed VCSELs with oxide aperture sizes of 8.3 μm (a), 6.6 μm (b), 4.6 μm (c). 1 V peak-to-peak modulation amplitude is used. The italic written bias currents represents subthreshold 0-state.

Pulse Distortion

To investigate the effects of turn-on delay and power overshoot on ultra-high-speed SDoF communication link, three studied VCSELs are operated at different bias currents with a constant input modulation amplitude V_{pp}=1 V. The measured digital pulse responses after the photo-receiver is presented in Fig. 4.4. As expected, impact of the turn-on delay and power overshoot is highest for the lowest bias current (green curves) since the 0-state is lowered with a lower bias current. The turn-on delay and power overshoot decreases and eventually disappears when the bias current is increased and this is due to the increasing level of the 0-state. Moreover, same bias currents result in different 0-state levels for different VCSELs. For example, when the 4.6 μm VCSEL is biased at 3 mA the 0-state is above the threshold, whereas for the 6.6 μm VCSEL same current results in subthreshold 0-state. The reason for this is the fact that the current swing of the larger aperture VCSEL is much higher than the smaller VCSEL, for the same voltage swing. The curves representing the highest bias currents (yellow curves) in Fig. 4.4 does not show any power overshoot or turn-on delay, indicating a well over threshold 0-state operation. Hence, the effect of pulse distortion is significantly decreased on SDoF communication link.

Effect on the Link Performance

The level of 0-state is not only dependent on the bias current but also the input modulation amplitude. To discover and quantify the effect of turn-on delay and power overshoot on SDoF-link performance, experiments with all three VCSELs are performed with different bias currents and input amplitudes. The calculated EVM of the captured symbols are presented in Fig. 4.5. The SDoF-link performance increases significantly for higher bias currents and lower input amplitudes, regardless of the employed VCSEL. This is an expected consequence of 0-state level being further away from the threshold, decreasing the pulse distortion caused by power overshoot and turn-on delay. Another important observation is that each VCSEL achieves a similar performance at the optimum operating point, which then the noise floor of the PPG becomes the
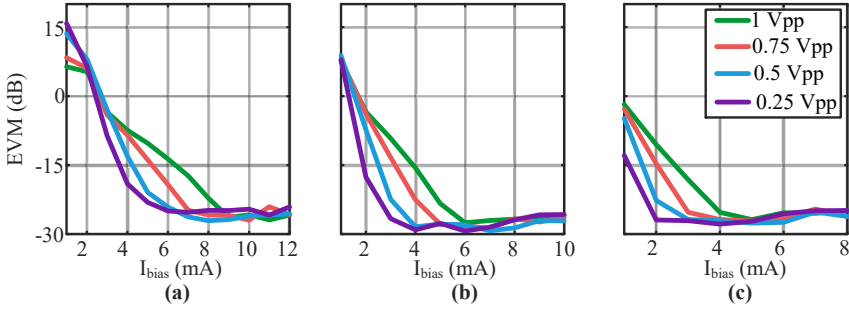
Figure 4.5: Calculated EVM values of the captured symbols for the three employed VCSELs with oxide aperture sizes of 8.3 μm (a), 6.6 μm (b), 4.6 μm (c).

main limitation of the communication link. Moreover, for a given bias current and modulation amplitude, smaller VCSELs exhibit less power overshoot and turn-on delay, see Fig. 4.5. The main reason for this is the fact that smaller volume results in a higher photon density inside the laser and therefore a higher damping of the relaxation oscillations and lower threshold current [79].

4.3.2   Energy Efficiency and Lifetime

Until so far in this chapter, it is shown that each VCSEL can achieve similar performance with certain bias current and input amplitude, see Fig. 4.5. Besides the performance of the communication link, the life span and the energy efficiency are also important properties. Energy efficiency and the life span of the VCSEL has an important role in this aspect [83], in datacom applications.

Energy Efficiency

In general, energy efficiency of a VCSEL can be calculated in three different ways: electrical energy-to-data-ratio (EDR), dissipated heat-to-bit rate ratio (HBR), and energy to data distance ratio (EDDR) [84]. In this work we studied HBR, defined by:

$$\text{HBR} = \frac{P_{\text{diss}}}{\text{BR}}, \tag{4.1}$$

where P_{diss} is the dissipated power and BR is the bit-rate. The dissipated power is computed by:

$$P_{\text{diss}} = P_{\text{el}} - P_{\text{opt}} \approx V_{\text{b}} \times I_{\text{b}} - P_{\text{opt,average}}, \tag{4.2}$$

where P_{el} and P_{opt} are the electrical power delivered to, and the optical output power from, the VCSEL, respectively. I_{b}, V_{b} and $P_{\text{opt,average}}$ represents the VCSEL bias current, bias voltage and average optical output power, respectively.

HBR for different bias currents for each VCSEL is presented in Fig. 4.6. As shown previously in Fig. 4.3 (b), smaller VCSELs have higher differential resistance and thereby higher voltage drop at larger bias currents compared to larger VCSELs. Consequently, smaller VCSELs becomes less efficient at larger bias currents, i.e. higher HBR. On the other hand, to reach a certain EVM
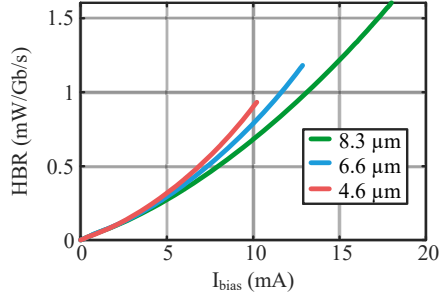
Figure 4.6: Heat-to-bitrate-ratio at 32 Gbps with respect to bias current for each VCSEL.

performance at the SDoF communication link, smaller VCSELs require smaller bias currents and therefore result in higher energy efficiency.

Lifetime

In cost sensitive applications, the lifetime of VCSELs plays a very important role in order to keep the maintaining cost as low as possible. Typically, the life time of a VCSEL required be longer than 10 years in such systems, which requires a maximum current density of of $J_{\max} = 10 \text{ kA/cm}^2$. The maximum current density inside the VCSEL is usually estimated via:

$$J_{\max} = \frac{I_{\text{bias}}}{A_{\text{ox}}},\tag{4.3}$$

where A_{ox} is the area of the oxide aperture. For the same bias current smaller VCSELs result in higher $J_{\max}$ hence shorter life span. However, as mentioned previously, smaller VCSELs provides better performance at lower currents due to the eased BER requirements of SDoF and lower pulse distortion caused by the turn-on delay and power overshoot. All the performance trade-offs are summarized in Table 4.1, where the the current density and HBR at the bias current required to reach the minimum EVM (-28 dB) is presented for each VCSEL. As shown in the table, the VCSEL having the smallest oxide aperture sizes of 4.6 μm, operating at 2 mA bias current and 0.25 V modulation voltage, can provide minimum EVM at a HBR of only 0.1 mW/Gb/s, while not exceeding a current density of 10 kA/cm^2. Thus, our results indicate that a high performance and energy efficient SDoF-link can be achieved, with long potential lifespan.

4.4 Potential and Limitations

After investigating the effects of VCSEL characteristics on SDoF communication link, the potential and the limitations of such links are explored in terms of the central frequency and the data rate.

4.4.1 Carrier Frequency

As mentioned in the previous chapter, SDoF systems benefit from flexible carrier frequencies enabled by the digital up-conversion stage. In this section

Table 4.1: Minimum bias current (Bias Cur.) for minimum EVM performance, i.e. EVM ~-28 dB for different modulation voltages and different VCSELs. For the given bias currents, maximum current density (Current Dens.) (kA/cm^2) inside the VCSELs and the heat-to-bitrate ratio (HBR) ($mW/Gb/s$) is also presented.

Modulation Voltage		Aperture Size		
		4.6 μm	6.6 μm	4.6 μm
0.25 V_{pp}	Bias Cur.	2	4	6
	Current Dens.	9.45	10.09	8.71
	HBR	0.10	0.22	0.34
0.5 V_{pp}	Bias Cur.	3	4	7
	Current Dens.	14.21	10.09	10.14
	HBR	0.16	0.22	0.42
0.75 V_{pp}	Bias Cur.	4	5	8
	Current Dens.	18.90	12.60	11.61
	HBR	0.23	0.29	0.50
1 V_{pp}	Bias Cur.	5	6	9
	Current Dens.	23.62	15.12	13.06
	HBR	0.27	0.38	0.59

the performance of an ultra-high speed SDoF communication link is investigated for different carrier frequencies. Signals centered at various carrier frequencies with 32 Gbps sigma-delta sampling rate, 250 Msym/s symbol rate and 64 QAM modulation are transmitted from a pulse-pattern-generator (PPG) (Anritsu MU183020A) and acquired by a high bandwidth oscilloscope (Tektronix DPO733304D). The calculated EVMs of demodulated symbols (Opt.) for different carrier frequencies are presented in Fig. 4.7 (a). Degrading performance for higher frequencies despite the theory [25], is due to the decreasing output power of the PPG (Pow.) and not caused by the SDoF components. This is further verified by acquiring the output of the PPG (El.) without the optical communication link, see Fig. 4.7 (a). Small EVM degradation observed at the optical link is caused by the relative-intensity-noise from the VCSEL and the thermal noise of the photo receiver.

4.4.2 Bit-Rate

Bitrate and signal quality performance of SDoF for different combinations of symbol rates and modulation formats are investigated. Combinations of three different modulation schemes (16, 64 and 256 QAM) and three different symbol rates (250, 500 and 1000 Msym/s) with 12 GHz carrier frequency are used, corresponding to bit rates 1-8 Gbps.

The results of the measurements are presented in Fig. 4.7 (b). As expected, increasing the modulation order does not effect the EVM performance, however it increases the bit-error rate. For a given SNR, larger modulation orders result in higher BER compared to the smaller ones, due to the condensed constellation points. Moreover, increasing the bandwidth results in EVM degradation and this is due to the constant power budget of the VCSEL. In other words, increasing the bandwidth decreases the in-band power of the sigma-delta modulated signal and with a constant noise floor it yields to a
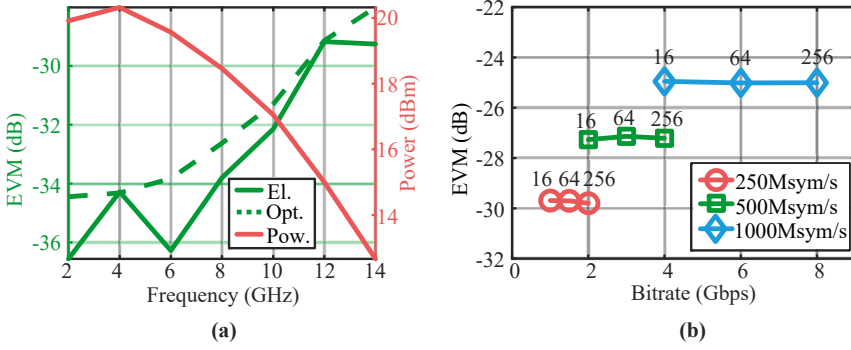
Figure 4.7: (a) EVM of captured symbols at the output of the photoreceiver (Opt.) and output of the pulse-pattern-generator (El.) for different center frequencies. 250 Msym/s symbol rate and 64 QAM modulation is used in order to isolate the effect of carrier frequency. The in-band output power of the pulse-pattern-generator with respect to center frequency is presented in the right axis. (b) Bitrate as function of modulation order and symbol rate. The numbers above the lines represents the modulation orders of 16, 64, 256 QAM.

higher EVM. Nevertheless, the results show that SDoF can be used to transmit a 8 Gbps modulated signal at 12 GHz carrier frequency with an EVM of -25 dB.

4.5   Discussion

In this chapter, potential and limitations of ultra-high-speed SDoF links with state-of-the-art VCSELs are investigated. First, the effects of VCSEL characteristics on such communication links are investigated by employing three different VCSELs. The signal quality of the SDoF communication link is evaluated under various bias currents and modulation voltages. Then, experiments with different carrier frequencies (2-14 Ghz) and bitrates (1-8 Gbps) are performed.

   The results indicate that ultra-high-speed SDoF communication links employing state-of-the-art VCSELs can be realized in beyond 10 GHz systems. The integration will not only enable low-cost, low-complexity RRHs, but also provide low-energy efficiency and long life span potential.

Chapter 5

Conclusions

In this thesis the potential and limitations of the sigma-delta-over-fiber communication technique have been investigated. The investigations are performed for both multiple-input-multiple-output (MIMO) and wide bandwidth, beyond 10 GHz communication systems.

MIMO is one of the key technologies behind the current (4G) and future generation (5G and beyond) mobile communication networks. Physically distributing the antenna elements/access points of a MIMO system is a method to increase the capacity and the coverage. However, the phase synchronization requirement of such distributed MIMO communication techniques requires extra measures due to the large distance between the access points. The existing D-MIMO implementations are designed for real-time communication and they are costly and complicated when it comes to the experimental studies. Hence, there is also a need for low-cost, low-complexity platforms aimed for initial and fundamental D-MIMO studies and experiments at an early stage. In this thesis, this problem is addressed and a novel method to form distributed MIMO communication systems is proposed by employing sigma-delta-over-fiber. The phase coherency and the performance of the testbed is evaluated through various measurements. The results show that the testbed is a low-complexity, low-cost, powerful platform to conduct measurements, research and analysis of distributed MIMO communication systems in real environments.

The need for larger bandwidths necessitates to use higher carrier frequencies than today. This results in increased number of central-stations and remote radio units. Forming the links between the central stations and remote units by SDoF is a promising method to keep the cost and complexity low. An ultra-high-speed SDoF communication link is realized with state-of-the-art vertical-cavity surface-emitting-lasers (VCSEL) in order to evaluate its maximum performance and applicability. The link performance and the power consumption are investigated with different VCSELs and various signals. The results showed that ultra-high-speed SDoF links employing low-cost, energy efficient VCSELs is a very strong candidate for carrier frequencies beyond 10 GHz.

This thesis presented the potential of sigma-delta-over-fiber technique as enabling low-cost, low-complexity, energy efficient, wide-bandwidth wireless communication networks.

5.1   Future Work

The following areas are interesting to explore in future research.

5.1.1   Up-link

Sigma-delta-over-fiber is mostly explored for down-link communication, since
there it enables low-complexity access points without any up-conversion stage.
In a system with SDoF downlink, conventional analog-radio-over-fiber can
form the up-link to the cost of sensitivity to non-linear distortion and dynamic
range [15]. This implementation maintains the low-complexity access points,
since the down-conversion of the received signal is performed at the central
unit. However, the complexity at the central station would remain high. In
order to eliminate the limitations of ARoF while keeping the complexity at
the access points low, a single-bit optical communication can be implemented.
This approach, requires a high sampling rate comparator to generate a digital
signal at the access point. This can be a very promising method, since it can
enable binary communication both for down- and up-link with low-complexity,
synchronized access points.

5.1.2   Pushing the Frequency Limits

The current state-of-the-art VCSELs can support 56 Gbps error-free binary
communication links [80]. Theoretically, this enables carrier frequencies up
to 28 GHz with sigma-delta-modulation. A SDoF communication link with
56 Gbps sampling rate can be very interesting to investigate for carrier frequen-
cies beyond 20 GHz.

Acknowledgments

I think this is one of the hardest parts of writing this thesis, expressing my gratitude to the people who supported me during my doctoral studies, I don't think I can find enough words to express my thankfulness. Nevertheless, I will try my best!

First of all, I would like to start with my examiner, the head of Microwave Electronics Laboratory, Prof. Herbert Zirath. Thank you for the opportunity to become a part of very inspiring group as Ph.D. student.

My deepest gratitude is to my main supervisor, Prof. Christian Fager, for his limitless support. No matter how busy you are with all the responsibilities you have, you always have time to supervise and have very fruitful discussions. I am very lucky, because I know I can always knock on your door and get your advice on anything. This hole journey has been very inspiring for me as becoming a researcher. Thank you!

I would like to thank Prof. Thomas Eriksson, my co-supervisor, for his support from the beginning of my doctoral studies. All our long, thorough discussions in signal processing field were very helpful. It is always relieving to know that I can have a meeting with you whenever I need!

Assoc. Prof. Johan Gustavsson, my co-supervisor, thank you very much for your time and your guidance about photonics and optical communication techniques. Your technical expertise improved the quality of my research.

Special thanks to Asst. Prof. Zhongxia Simon He. I really appreciate our discussions and your guidance. It is always a pleasure to discuss with you regardless of the topic.

I am particularly grateful to my colleagues for creating such a welcoming and fun working environment.

Necla, you were there to support me every single time I struggled in my life. I could write a book to acknowledge you, yet I need to express my gratitude in couple of lines. So, I prefer to say, I love you!

I don't think there are enough words to express my gratitude to my parents. Their support throughout my life enabled me to write a licentiate thesis. Melahat and Umit, thank you very much!

Bibliography

[1] "Ericsson Mobility Report," Ericsson AB, Tech. Rep., November 2018.

[2] D. Novak, R. B. Waterhouse, A. Nirmalathas, C. Lim, P. A. Gamage, T. R. Clark, M. L. Dennis, and J. A. Nanzer, "Radio-over-fiber technologies for emerging wireless systems," *IEEE J. Quantum Electron.*, vol. 52, no. 1, pp. 1–11, Jan 2016.

[3] D. M. Fye, "Design of fiber optic antenna remoting links for cellular radio applications," in *40th IEEE Conference on Vehicular Technology*, May 1990, pp. 622–625.

[4] A. J. Cooper, "'fibre/radio' for the provision of cordless/mobile telephony services in the access network," *Electronics Letters*, vol. 26, no. 24, pp. 2054–2056, Nov 1990.

[5] A. J. Seeds and K. J. Williams, "Microwave photonics," *J. Lightw. Technol*, vol. 24, no. 12, pp. 4628–4641, Dec 2006.

[6] A. Nirmalathas, P. A. Gamage, C. Lim, D. Novak, and R. Waterhouse, "Digitized radio-over-fiber technologies for converged optical wireless access network," *J. Lightw. Technol*, vol. 28, no. 16, pp. 2366–2375, Aug 2010.

[7] G. Chang, A. Chowdhury, , and G. Ellinas, "Architectures and technologies for very high throughput in-building wireless services using radio-over-fiber networks," in *2009 IEEE/LEOS Summer Topical Meeting*, July 2009, pp. 37–38.

[8] R. M. Borges, T. R. R. Marins, M. S. B. Cunha, H. R. D. Filgueiras, I. F. da Costa, R. N. da Silva, D. H. Spadoti, L. L. Mendes, and A. C. Sodré, "Integration of a GFDM-based 5G transceiver in a GPON using radio over fiber technology," *J. Lightw. Technol.*, vol. 36, no. 19, pp. 4468–4477, Oct 2018.

[9] Y. Li, I. A. Hemadeh, M. El-Hajjar, and L. Hanzo, "Radio over diber downlink design for spatial modulation and multi-set space-time shift-keying," *IEEE Access*, vol. 6, pp. 21 812–21 827, 2018.

[10] A. Delmade, C. Browning, A. Farhang, N. Marchetti, L. E. Doyle, R. D. Koilpillai, L. P. Barry, and D. Venkitesh, "Performance analysis of analog IF over fiber fronthaul link with 4G and 5G coexistence," *IEEE J. Opt. Commun. Netw*, vol. 10, no. 3, pp. 174–182, March 2018.

[11] J. Nanni, J. Polleux, C. Algani, S. Rusticelli, F. Perini, and G. Tartarini, "VCSEL-based radio-over-G652 fiber system for short-/medium-range MFH solutions," *J. Lightw. Technol*, vol. 36, no. 19, pp. 4430–4437, Oct 2018.

[12] M. Noweir, Q. Zhou, A. Kwan, R. Valivarthi, M. Helaoui, W. Tittel, and F. M. Ghannouchi, "Digitally linearized radio-over-fiber transmitter architecture for cloud radio access network's downlink," *IEEE Trans. Microw. Theory Techn.*, vol. 66, no. 7, pp. 3564–3574, July 2018.

[13] C. Lim, A. Nirmalathas, M. Bakaul, P. Gamage, K. Lee, Y. Yang, D. Novak, and R. Waterhouse, "Fiber-wireless networks and subsystem technologies," J. *Lightw. Technol.*, vol. 28, no. 4, pp. 390–405, Feb 2010.

[14] T. Kurniawan, A. Nirmalathas, C. Lim, D. Novak, and R. Waterhouse, "Performance analysis of optimized millimeter-wave fiber radio links," *IEEE Trans. Microw. Theory Techn.*, vol. 54, no. 2, pp. 921–928, Feb 2006.

[15] C. Lim, A. Nirmalathas, K. Lee, D. Novak, and R. Waterhouse, "Inter-modulation distortion improvement for fiber amp;ndash;radio applications incorporating OSSB+C modulation in an optical integrated-access environment," *J. Lightw. Technol.*, vol. 25, no. 6, pp. 1602–1612, June 2007.

[16] U. Gliese, S. Norskov, and T. N. Nielsen, "Chromatic dispersion in fiber-optic microwave and millimeter-wave links," *IEEE Trans. Microw. Theory Techn.*, vol. 44, no. 10, pp. 1716–1724, Oct 1996.

[17] P. A. Gamage, A. Nirmalathas, C. Lim, D. Novak, and R. Waterhouse, "Design and analysis of digitized RF-over-fiber links," *J. Lightw. Technol.*, vol. 27, no. 12, pp. 2052–2061, June 2009.

[18] A. Nirmalathas, P. A. Gamage, C. Lim, D. Novak, R. Waterhouse, and Y. Yang, "Digitized RF transmission over fiber," *IEEE Microwave Magazine*, vol. 10, no. 4, pp. 75–81, June 2009.

[19] "Open base station architecture initiative." [Online]. Available: http://www.obsai.com/

[20] "Common public radio interface." [Online]. Available: http://www.cpri.info/

[21] D. M. Akos, M. Stockmaster, J. B. Y. Tsui, and J. Caschera, "Direct bandpass sampling of multiple distinct RF signals," *IEEE Trans. Commun.*, vol. 47, no. 7, pp. 983–988, July 1999.

[22] H. Jung, K. W. Lee, J. Kim, Y. Kwon, and J. H. Park, "Performance comparison of analog and digitized RoF systems with nonlinear channel condition," *IEEE Photon. Technol. Lett.*, vol. 28, no. 6, pp. 661–664, March 2016.

[23] L. M. Pessoa, J. S. Tavares, D. Coelho, and H. M. Salgado, "Experimental evaluation of a digitized fiber-wireless system employing sigma delta modulation," *Optics Express*, vol. 22, no. 14, p. 17508, jul 2014.

[24] L. Breyne, G. Torfs, X. Yin, P. Demeester, and J. Bauwelinck, "Comparison between analog radio-over-fiber and sigma delta modulated radio-over-fiber," *IEEE Photon. Technol. Lett.*, vol. 29, no. 21, pp. 1808–1811, Nov 2017.

[25] R. Schreier and G. C. Temes, *Understanding Delta-Sigma Data Converters*, 1st ed. Hoboken N.J: John Wiley & Sons, 2004.

[26] S. Hein and A. Zakhor, "On the stability of sigma delta modulators," *IEEE Trans. Signal Process.*, vol. 41, pp. 2322–2348, 1993.

[27] W. L. Lee, "A novel higher order interpolative modulator topology for high resolution oversampling A/D converters," Master's thesis, Massachusetts Institute of Technology, Cambridge, MA, 1987.

[28] K. C. . Chao, S. Nadeem, W. L. Lee, and C. G. Sodini, "A higher order topology for interpolative modulators for oversampling A/D converters," *IEEE Transactions on Circuits and Systems*, vol. 37, no. 3, pp. 309–318, March 1990.

[29] S. Jang, G. Jo, J. Jung, B. Park, and S. Hong, "A digitized IF-over-fiber transmission based on low-pass delta-sigma modulation," *IEEE Photon. Technol. Lett.*, vol. 26, no. 24, pp. 2484–2487, Dec 2014.

[30] A. Lorences-Riesgo, S. S. Pereira, D. C. Dinis, J. Vieira, A. S. R. Oliveira, and P. P. Monteiro, "Real-time FPGA-based delta-sigma-modulation transmission for 60 GHz radio-over-fiber fronthaul," in *2018 European Conference on Optical Communication (ECOC)*, Sep. 2018, pp. 1–3.

[31] J. M. B. Oliveira, L. M. Pessoa, D. Coelho, J. S. Tavares, and H. M. Salgado, "Digitised radio techniques for fibre-wireless applications," in *2014 16th International Conference on Transparent Optical Networks (ICTON)*, July 2014, pp. 1–4.

[32] S. Hori, T. Yamase, M. Tanio, T. Kaneko, N. Tawa, K. Motoi, and K. Kunihiro, "A digital radio-over-fiber downlink system based on envelope delta-sigma modulation for multi-band/mode operation," in *2016 IEEE MTT-S International Microwave Symposium (IMS)*, May 2016, pp. 1–4.

[33] R. F. Cordeiro, A. S. R. Oliveira, and J. Vieira, "All-digital transmitter with RoF remote radio head," in *2014 IEEE MTT-S International Microwave Symposium (IMS2014)*, June 2014, pp. 1–4.

[34] C. Wu, H. Li, J. Van Kerrebrouck, L. Breyne, L. Bogaert, P. Demeester, and G. Torfs, "Real-time4 × 3.5Gbps sigma delta radio-over-fiber for a low-cost 5G C-RAN downlink," in *2018 European Conference on Optical Communication (ECOC)*, Sep. 2018, pp. 1–3.

[35] J. Wang, Z. Yu, K. Ying, J. Zhang, F. Lu, M. Xu, L. Cheng, X. Ma, and G. Chang, "Digital mobile fronthaul based on delta-sigma modulation for 32 LTE carrier aggregation and FBMC signals," *IEEE J. Opt. Commun. Netw*, vol. 9, no. 2, pp. A233–A244, Feb 2017.

[36] J. Wang, Z. Jia, L. A. Campos, L. Cheng, C. Knittle, and G. Chang, "Delta-sigma digitization and optical coherent transmission of DOCSIS 3.1 signals in hybrid fiber coax networks," *J. Lightw. Technol.*, vol. 36, no. 2, pp. 568–579, Jan 2018.

[37] A. Frappe, A. Flament, B. Stefanelli, A. Kaiser, and A. Cathelin, "An all-digital RF signal generator using high-speed $\Delta\Sigma$ modulators ," *IEEE J. Solid-State Circuits*, vol. 44, no. 10, pp. 2722–2732, Oct 2009.

[38] M. Ebrahimi, M. Helaoui, and F. Ghannouchi, "Time-interleaved delta-sigma modulator for wideband digital GHz transmitters design and SDR applications," *Progress In Electromagnetics Research B*, vol. 34, pp. 263–281, 2011.

[39] T. Canning, P. J. Tasker, and S. C. Cripps, "Continuous mode power amplifier design using harmonic clipping contours: Theory and practice," *IEEE Trans. Microw. Theory Techn.*, vol. 62, no. 1, pp. 100–110, Jan 2014.

[40] A. Paulraj, R. Nabar, and D. Gore, *Introduction to Space-time Wireless Communications*.   Cambridge University Press, 2003.

[41] A. Hadden, "Mobile broadband - where the next generation leads us [Industry Perspectives," *IEEE Wireless Communications*, vol. 16, no. 6, pp. 6–9, dec 2009.

[42] E. Ezhilarasan and M. Dinakaran, "A review on mobile technologies: 3G, 4G and 5G," in *2017 Second International Conference on Recent Trends and Challenges in Computational Models (ICRTCCM)*.   IEEE, feb 2017, pp. 369–373.

[43] J. G. Andrews, S. Buzzi, W. Choi, S. V. Hanly, A. Lozano, A. C. K. Soong, and J. C. Zhang, "What will 5G be?" *IEEE J. Sel. Areas Commun.*, vol. 32, no. 6, pp. 1065–1082, June 2014.

[44] D. Chizhik, G. Foschini, M. Gans, and R. Valenzuela, "Keyholes, correlations, and capacities of multielement transmit and receive antennas," *IEEE Trans. Wireless Commun.*, vol. 1, no. 2, pp. 361–368, apr 2002.

[45] Chen-Nee Chuah, J. Kahn, and D. Tse, "Capacity of multi-antenna array systems in indoor wireless environment," in *IEEE GLOBECOM 1998 (Cat. NO. 98CH36250)*, vol. 4.   IEEE, pp. 1894–1899.

[46] A. Saleh, A. Rustako, and R. Roman, "Distributed antennas for indoor radio communications," *IEEE Trans. Commun*, vol. 35, no. 12, pp. 1245–1251, dec 1987.

[47] M. Clark, T. Willis, L. Greenstein, A. Rustako, V. Erceg, and R. Roman, "Distributed versus centralized antenna arrays in broadband wireless networks," in *IEEE VTS 53rd Vehicular Technology Conference, Spring 2001. Proceedings (Cat. No.01CH37202)*, vol. 1.   IEEE, pp. 33–37.

[48] Shidong Zhou, Ming Zhao, Xibin Xu, Jing Wang, and Yan Yao, "Distributed wireless communication system: a new architecture for future public wireless access," *IEEE Communications Magazine*, vol. 41, no. 3, pp. 108–113, mar 2003.

[49] Wonil Roh and A. Paulraj, "Outage performance of the distributed antenna systems in a composite fading channel," in *Proceedings IEEE 56th Vehicular Technology Conference*, vol. 3.   IEEE, pp. 1520–1524.

[50] ——, "MIMO channel capacity for the distributed antenna," in *Proceedings IEEE 56th Vehicular Technology Conference*, vol. 2.   IEEE, pp. 706–709.

[51] Z. Liu and L. Dai, "A comparative study of downlink MIMO cellular networks with co-located and distributed base-station antennas," *IEEE Trans. Wireless Commun.*, vol. 13, no. 11, pp. 6259–6274, nov 2014.

[52] H. Q. Ngo, A. Ashikhmin, H. Yang, E. G. Larsson, and T. L. Marzetta, "Cell-free massive MIMO versus small cells," *IEEE Trans. Wireless Commun.*, vol. 16, no. 3, pp. 1834–1850, mar 2017.

[53] H. V. Balan, R. Rogalin, A. Michaloliakos, K. Psounis, and G. Caire, "AirSync: Enabling distributed multiuser MIMO with full spatial multiplexing," *IEEE/ACM Trans. Netw.*, vol. 21, no. 6, pp. 1681–1695, dec 2013.

[54] H. Rahul, S. Kumar, and D. Katabi, "MegaMIMO: Scaling Wireless Capacity with User Demands," in *ACM SIGCOMM 2012*, Helsinki, Finland, August 2012.

[55] X. Zhang, K. Sundaresan, M. A. A. Khojastepour, S. Rangarajan, and K. G. Shin, "NEMOx: Scalable network MIMO for wireless networks," in *Proceedings of the 19th Annual International Conference on Mobile Computing & Networking*, ser. MobiCom '13.   New York, NY, USA: ACM, 2013, pp. 453–464.

[56] V. Yenamandra and K. Srinivasan, "Vidyut: Exploiting power line infrastructure for enterprise wireless networks," in *Proceedings of the 2014 ACM Conference on SIGCOMM*, ser. SIGCOMM '14.   New York, NY, USA: ACM, 2014, pp. 595–606.

[57] E. Hamed, H. Rahul, M. A. Abdelghany, and D. Katabi, "Real-time distributed MIMO systems," in *Proceedings of the 2016 ACM SIGCOMM Conference*, ser. SIGCOMM '16.   New York, NY, USA: ACM, 2016, pp. 412–425.

[58] "Rice University WARP Project," 2012.

[59] "USRP, http://www.ettus.com, Ettus Inc."

[60] "Zedboard, http://zedboard.org , AVNET."

[61] "AD-FMCOMMS-EBZ, http://www.analog.com , Analog Devices."

[62] "NI-5791, http://www.ni.com, National Instruments."

[63] "Zinwave, http://www.zinwave.com , Zinwave."

[64] "pCell, https://www.artemis.com/pcell , Artemis."

[65] A. Jerng and C. G. Sodini, "A wideband delta-sigma digital-RF modulator for high data rate transmitters," *IEEE J. Solid-State Circuits*, vol. 42, no. 8, pp. 1710–1722, Aug 2007.

[66] M. Helaoui, S. Hatami, R. Negra, and F. M. Ghannouchi, "A novel architecture of delta-sigma modulator enabling all-digital multiband multistandard RF transmitters design," *IEEE Trans. Circuits Syst., II, Exp. Briefs*, vol. 55, no. 11, pp. 1129–1133, Nov 2008.

[67] D. C. Dinis, A. S. R. Oliveira, and J. Vieira, "All-digital transmitter based antenna array with reduced hardware complexity," in *2017 IEEE MTT-S International Microwave Symposium (IMS)*, June 2017, pp. 153–156.

[68] M. Tanio, S. Hori, N. Tawa, T. Kuwabara, and K. Kunihiro, "An FPGA-based 1-bit digital transmitter with 800-MHz bandwidth for 5G millimeter-wave active antenna systems," in *2018 IEEE/MTT-S International Microwave Symposium - IMS*, June 2018, pp. 499–502.

[69] D. C. Dinis, R. Ma, K. H. Teo, P. Orlik, A. S. R. Oliveira, and J. Vieira, "An FPGA-based multi-level all-digital transmitter with 1.25 GHz of bandwidth," in *2018 IEEE/MTT-S International Microwave Symposium - IMS*, June 2018, pp. 659–662.

[70] G. Caire and S. Shamai, "On the achievable throughput of a multiantenna Gaussian broadcast channel," *IEEE Trans. Inf. Theory*, vol. 49, no. 7, pp. 1691–1706, jul 2003.

[71] ——, "On the achievable throughput of a multiantenna Gaussian broadcast channel," *IEEE Trans. Inf. Theory*, vol. 49, no. 7, pp. 1691–1706, July 2003.

[72] K. Iga, "Surface-emitting laser-its birth and generation of new optoelectronics field," *IEEE J. Sel. Topics Quantum Electron*, vol. 6, no. 6, pp. 1201–1215, Nov 2000.

[73] D. K. Serkland, G. M. Peake, K. M. Geib, R. Lutwak, R. M. Garvey, M. Varghese, and M. Mescher, "VCSELs for atomic clocks," in *Vertical-Cavity Surface-Emitting Lasers X*, ser. Proc.SPIE, C. Lei and K. D. Choquette, Eds., vol. 6132, Feb. 2006, pp. 66–76.

[74] *VCSEL array-based light exposure system for laser printing*, vol. 6908, 2008.

[75] A. Extance, "Faces light up over VCSEL prospects," *SPIE Newsroom*, Apr. 2018.

[76] G. Totschnig, M. Lackner, R. Shau, M. Ortsiefer, J. Rosskopf, M. Amann, and F. Winter, "High-speed vertical-cavity surface-emitting laser (vcsel) absorption spectroscopy of ammonia (nh3) near 1.54 μm," *Applied Physics B*, vol. 76, no. 5, pp. 603–608, May 2003.

[77] *Volume production of polarization controlled single-mode VCSELs*, vol. 6908, 2008.

[78] F. Koyama, "Recent advances of VCSEL photonics," *J. Lightw. Technol.*, vol. 24, no. 12, pp. 4502–4513, Dec 2006.

[79] P. Westbergh, R. Safaisini, E. Haglund, J. S. Gustavsson, A. Larsson, M. Geen, R. Lawrence, and A. Joel, "High-speed oxide confined 850-nm VCSELs operating error-free at 40 Gb/s up to 85 C," *IEEE Photon. Technol. Lett*, vol. 25, no. 8, pp. 768–771, apr 2013.

[80] P. Westbergh, E. Haglund, E. Haglund, R. Safaisini, J. Gustavsson, and A. Larsson, "High-speed 850 nm VCSELs operating error free up to 57 Gbit/s," *Electronics Letters*, vol. 49, no. 16, pp. 1021–1023, aug 2013.

[81] J. A. Tatum, D. Gazula, L. A. Graham, J. K. Guenter, R. H. Johnson, J. King, C. Kocot, G. D. Landry, I. Lyubomirsky, A. N. MacInnes, E. M. Shaw, K. Balemarthy, R. Shubochkin, D. Vaidya, M. Yan, and F. Tang, "VCSEL-based interconnects for current and future data centers," *J. Lightw. Technol.*, vol. 33, no. 4, pp. 727–732, Feb 2015.

[82] X. Zhang, W. Pan, J. Chen, and H. Zhang, "Theoretical calculation of turn-on delay time of VCSEL and effect of carriers recombination," *Optics & Laser Technology*, vol. 39, no. 5, pp. 997–1001, jul 2007.

[83] W. H. Hofmann, P. Moser, and D. Bimberg, "Energy-efficient VCSELs for interconnects," *IEEE Photon. J.*, vol. 4, no. 2, pp. 652–656, April 2012.

[84] P. Moser, J. A. Lott, and D. Bimberg, "Energy efficiency of directly modulated oxide-confined high bit rate 850-nm VCSELs for optical interconnects," *IEEE J. Sel. Topics Quantum Electron*, vol. 19, no. 4, pp. 1 702 212–1 702 212, jul 2013.